

NASA Technical Memorandum 102165

JOHNSON
IN-26
1662
P64

Behavior of Surface and Corner Cracks Subjected to Tensile and Bending Loads in Ti-6Al-4V Alloy

Royce G. Forman
Sambi R. Mettu

September 1990

(NASA-TM-102165) BEHAVIOR OF SURFACE AND
CORNER CRACKS SUBJECTED TO TENSILE AND
BENDING LOADS IN Ti-6Al-4V ALLOY (NASA)
64 D CSCL 11F

N91-19273

Unclas
G3/26 0001662



•

•

•

•

•

•

•

•

•

•

NASA Technical Memorandum 102165

Behavior of Surface and Corner Cracks
Subjected to Tensile and Bending Loads
in Ti-6Al-4V Alloy

Royce G. Forman
*Lyndon B. Johnson Space Center
Houston, Texas*

Sambi R. Mettu
*Lockheed Engineering and Sciences Company
Houston, Texas*

National Aeronautics and Space Administration
Lyndon B. Johnson Space Center
Houston, Texas

September 1990

medieval and modernist. We have seen that the medieval

Contents

Section	Page
Abstract	1
Introduction	1
Details of Experiments	2
Analytical Predictions	4
Discussion	7
Conclusions	8
References	9

Tables

Table	Page
1 Tensile Test Data for Ti-6Al-4V	10
2 A Typical Heat-tint Schedule	10
3 Plane-Strain Fracture Toughness from C(T) Specimens	11
4 Fracture Toughness from Surface-Cracked Rectangular Specimens .	12
5 Fracture Toughness from Surface-Cracked Round Specimens	14
6 Fracture Toughness from Surface-Cracked Threaded Round Specimens	15
7 Fracture Toughness from Corner-Cracked Rectangular Specimens .	16
8 Fracture Toughness from Corner-Cracked Rectangular Specimens (Open Hole)	17
9 Fracture Toughness from Corner-Cracked Rectangular Specimens (Open Hole)	18
10 Basic Crack Growth Constants Used for Life Prediction in Ti-6Al-4V	19
11 Life Prediction for SC01	20
12 Life Prediction for SC07	21
13 Life Prediction for SC08	22
14 Life Prediction for CC01	23
15 Life Prediction for CC02	24
16 Life Prediction for CC03	26

Figures

Figure		Page
1	Summary of fracture toughness results	27
2	Summary of fracture toughness results	28
3	Crack surfaces showing heat-tint marks	29
4	Base curve fit of fatigue crack growth rates, data from standard specimens	32
5	Comparison of fatigue crack growth rates, surface crack in rectangular bar - tension	33
6	Comparison of fatigue crack growth rates, surface crack in rectangular bar - three-point bending	34
7	Comparison of fatigue crack growth rates, surface crack in rectangular bar - cantilever bending	35
8	Comparison of fatigue crack growth rates, surface crack in a round bar - tension	36
9	Comparison of fatigue crack growth rates, surface crack in a round bar - bending	37
10	Comparison of fatigue crack growth rates, surface crack in threaded round bar - tension	38
11	Comparison of fatigue crack growth rates, surface crack in threaded round bar - bending	39
12	Comparison of fatigue crack growth rates, corner crack in rectangular bar - tension	40
13	Comparison of fatigue crack growth rates, corner crack in rectangular bar - bending	41
14	Comparison of fatigue crack growth rates, corner crack in rectangular bar - bending	42
15	Comparison of fatigue crack growth rates, corner cracked rectangular bar - transverse bending	43
16	Comparison of fatigue crack growth rates, corner crack from open hole rectangular bar - tension	44
17	Comparison of fatigue crack growth rates, corner crack from open hole, rectangular bar - 3-point bending	45
18	Comparison of fatigue crack growth rates, corner crack from open hole, rectangular bar - 3-point bending	46

Figures (concluded)

Figure		Page
19	Comparison of fatigue crack growth rates, corner crack from open hole, rectangular bar - 3-point bending	47
20	Comparison of fatigue crack growth rates, corner crack from open hole, rectangular bar - 3-point bending	48
21	Comparison of fatigue crack growth rates, corner crack from pin-loaded hole, rectangular bar	49
22	Comparison of fatigue crack growth rates, corner crack from pin-loaded hole, rectangular bar	50
23	Comparison of fatigue crack growth rates, corner crack from pin-loaded hole, rectangular bar	51
24	Comparison of fatigue crack growth rates, corner crack from pin-loaded hole, rectangular bar	52
25	Summary of life prediction results	53
26	Summary of life prediction results	54
27	Stress concentration factor for a plate with a corner crack from hole in bending	55
28	Empirical stress intensity correction factor for a corner crack from hole in bending	56
29	Fracture toughness vs crack depth parameter for a surface crack	57
30	Net-section stress ratio vs crack depth parameter for a surface crack	58



Behavior of Surface and Corner Cracks Subjected to Tensile and Bending Loads in Ti-6Al-4V Alloy

Royce G. Forman

Lyndon B. Johnson Space Center

and

Sambi R. Mettu

Lockheed Engineering and Sciences Company

Abstract

The behavior of part-through flaws with regard to failure under monotonic loading and their growth under fatigue loading was investigated experimentally and analytically. The objective of this memorandum is to present comparisons of experimental values of toughness obtained using surface- and corner-cracked specimens with those obtained using standard test specimens, and also to compare experimental growth cycles with numerical predictions using the NASA/FLAGRO computer program. Tests were conducted on various types of surface and corner cracks under tensile and bending loads. Room temperature laboratory air provided the test environment. The material used in this investigation was the Ti-6Al-4V alloy in the solution treated and aged (STA) and stress-relieved condition. Detailed tabulation of the fracture toughness data and results of life prediction using the NASA/FLAGRO program are presented. Fatigue crack growth rates for the part-through-cracked specimens are compared with a base curve fitted from the data obtained using standard specimens. The fatigue loading used in the crack growth testing was of constant-amplitude sinusoidal type. It is concluded that the fatigue crack growth rates from standard specimens can be used with reasonable accuracy in the case of surface and corner cracks, but the fracture toughness values from standard specimens are too conservative for the surface- and corner-crack cases.

Introduction

The behavior of surface and corner cracks needs to be adequately understood to make meaningful failure predictions in real structures. This is because such part-through cracks occur more often and the behavior witnessed is more complex than for through-type crack problems. The American Society for Testing and Materials (ASTM) Standard Test Method E-399 for Plane-Strain Fracture Toughness of Metallic Materials uses through-cracked specimens such as the compact tension (C(T)), arc-shaped tension, disk-shaped tension, or the single-edge notched bend specimen and is aimed at establishing the lower bound on toughness for a given material. Also, the ASTM Standard Test Method E-647 for Measurement

of Fatigue Crack Growth Rates recommends using through-cracked specimens such as C(T) or the middle-cracked tension (M(T)). However, in real structures, in addition to through cracks, a common type of flaw is part-through. Idealized shapes of these flaws may be treated as semi-elliptical at a surface or quarter-elliptical at a corner. Owing to the lesser constraint on plastic deformation in these crack cases, the fracture toughness is likely to be higher than the standard plane-strain value. At present, there is no standard test method which uses such practically important configurations. In order to use the data from the standard test methods for predictions involving part-through flaws, one needs to explore if specimens containing part-through cracks produce results similar to those containing through cracks. The present investigation was directed at obtaining the linear elastic fracture toughness from part-through-cracked specimens experimentally and comparing it with the toughness obtained using the standard through-cracked specimens. In other words, the objective was to determine the degree of conservatism in using plane-strain fracture toughness in place of the actual toughness from part-through-cracked specimens. Also, the investigation was aimed at measuring the crack growth rates and growth cycles of various specimens subjected to constant-amplitude loading. The measured crack-growth cycles were compared with analytically predicted cycles using the software program NASA/FLAGRO.

A recent study by Reuter[1] addresses comparison of the plane-strain fracture toughness with the toughness obtained using surface-cracked specimens for two materials, a ceramic (SiC) and a titanium alloy (Ti-15-3). Another study related to the present study (also by Forman *et al.*[2]) concentrates on the fracture properties of a beryllium-copper (Be-Cu) alloy. The fracture toughness values obtained using the C(T) specimens were compared with those from surface-cracked and center-cracked specimens. A limited comparison of crack growth data from C(T) and corner-cracked specimens made of Ti-6Al-4V was done by Kalluri and Telesman[3] which shows no substantial difference between the growth rates from the two types of specimens.

Details of Experiments

The material used in this investigation was the titanium alloy Ti-6Al-4V. All specimens were made from the same batch of 1-in. thick bar stock in the STA condition and stress relieved (SR). The basic strength properties were determined using dog-bone-type specimens. The results of the tensile tests are summarized in table 1. The plane-strain fracture toughness values were determined using two C(T) specimens having the L-T orientation and three specimens having the T-L orientation. Both C(T) and the single-edge-notched bend (SE(B)) specimens were used for obtaining the basic fatigue crack growth (FCG) data. Six types of part-through-cracked specimens were used for FCG and fracture toughness testing. They were

- . Rectangular bars with surface cracks (SC01),
- . Smooth round bars with thumb-nail surface cracks (SC07),
- . Threaded round bars with surface cracks at thread roots (SC08),
- . Rectangular bars with corner cracks (CC01),
- . Rectangular bars with corner cracks from open holes (CC02), and
- . Rectangular bars with corner cracks from pin-loaded holes (CC03).

These crack configurations are illustrated in figures 1, 2, and 3. With the exception of the pin-loaded hole, all specimens were subjected to both tensile and bending loads.

Starter notches were introduced in all the specimens by the electro-discharge machining (EDM) method. The specimens were then subjected to constant-amplitude fatigue loading in servo-hydraulic test machines. The EDM notch was allowed to grow into the shape of a semi- or quarter-ellipse before starting the actual cycle-counting for the purpose of growth-rate computations. Crack-growth measurements were performed using an optical microscope on the broken specimen halves after each test was completed. Specimens were viewed at a magnification of 10 X and the microscope had a least count of 0.0001 in. Heat-tinting technique was used to mark the position of the growing cracks after every few hundred cycles of loading. In this technique, the test is stopped after some known number of cycles; the specimen is soaked at a particular temperature for a particular period of time, and cooled in laboratory air to room temperature; and the test is resumed. The method produces different colored tints for different soaking temperatures and soaking times on the crack face, thus showing the position of the crack after various number of cycles during the fatigue loading. Figures 3(a), 3(b), and 3(c) show photo-scanned views of the specimens having tinted crack surfaces. For each crack case, a sample of the tensile loading and bending loading are shown. Table 2 shows a set of typical temperatures and corresponding soaking times for producing the tints.

After sufficient crack growth occurred under fatigue loading, most specimens were monotonically loaded either in tension or in bending until failure to obtain fracture toughness values. In a few cases, failure occurred during the fatigue cycling itself; in which case the maximum load value during the cycle was used as the failure load. Thus, from each specimen, about four or five points on the crack growth curve were obtained. By using different load levels, the values of crack growth rate were obtained over a wide range of the stress intensity factor range ΔK . The a vs N data from the tests were converted to da/dN using a simple forward-difference technique. This is described by the general equation

$$(da/dN)_i = \frac{a_{i+1} - a_i}{N_{i+1} - N_i} \quad (1)$$

thus generating i values of da/dN for $(i+1)$ points of a vs N . A similar procedure is applied to the crack growth dc/dN in the width direction. Corresponding ranges of the stress intensity factor ΔK were calculated using the NASA/FLAGRO program.

Analytical Predictions

Stress intensity factors for the part-through-cracked specimens were computed using the relevant crack case in the NASA/FLAGRO computer program [4]. This software program has been in use by the aerospace community since 1986. It is a comprehensive program useful for computing the elastic stress intensity factors for a number of crack configurations and to compute the crack growth under fatigue loading so that safe-life predictions can be made. The program is user-friendly and has a number of other features useful for fracture mechanics analyses. It is being continually improved by incorporating new stress intensity solutions as well as implementing new algorithms for crack growth predictions under spectrum loading. The measured values of crack lengths a and c and the failure loads were used to compute the fracture toughness for various specimens. Details of the stress intensity factor solutions as well as the references they were taken from are given in [4].

The plane-strain fracture toughness (K_{Ic}) from two C(T) specimens averaged to about $50 \text{ ksi}\sqrt{\text{in.}}$ for the L-T grain-orientation and about $42 \text{ ksi}\sqrt{\text{in.}}$ for the T-L orientation. Table 3 shows the details. The toughness values from the surface and corner cracks (K_{Ic}) are all summarized in figures 1 and 2. It was found that the K_{Ic} values were significantly higher than the K_{Ic} values. Detailed tabulation of the specimen dimensions, failure loads and calculated toughness values for all the specimens are shown in tables 4 to 9. These tables give an idea of the consistency (or scatter as the case may be) among the test data. More comments on these results are included in the discussion section.

In order to predict the crack growth life, the basic curve fit parameters needed by NASA/FLAGRO were obtained from crack growth tests on standard compact and bend specimens. These data were then curve-fitted to the Forman-Newman-de Koning(FNK) crack growth law[4] given by

$$\frac{da}{dN} = \frac{C(1-f)^n \Delta K^n \left(1 - \frac{\Delta K_{th}}{\Delta K}\right)^p}{(1-R)^n \left(1 - \frac{\Delta K}{(1-R)K_c}\right)^q} \quad (2)$$

In the above equation, a is the crack depth, N is the number of cycles of constant-amplitude loading, f is a crack-opening function empirically formulated by Newman[5], R is the ratio of minimum to maximum load in a cycle, ΔK is the stress intensity factor range, ΔK_{th} is the threshold stress intensity range, K_c is the fracture toughness and C, n, p, q are empirical constants. The crack opening function f is defined by[5]

$$f = K_{op}/K_{max} = A_0 + A_1R + A_2R^2 + A_3R^3, \quad R \geq 0 \quad (3)$$

and

$$f = K_{op}/K_{max} = A_0 + A_1R, \quad -1 \leq R < 0 \quad (4)$$

The opening stress intensity factor K_{op} is assumed to be greater than the minimum applied stress intensity K_{min} during a cycle of loading. The coefficients A_0 to A_3 are functions of the maximum stress level ratio S_{max}/σ_o and the constraint factor α . σ_o is the flow stress which is the average of the yield and ultimate stresses, and α varies from 1 for plane stress to 3 for plane strain. The coefficients are

$$A_0 = (0.825 - 0.34\alpha + 0.05\alpha^2)[\cos(\pi S_{max}/2\sigma_o)]^{1/\alpha} \quad (5)$$

$$A_1 = (0.415 - 0.071\alpha)S_{max}/\sigma_o \quad (6)$$

$$A_2 = 1 - A_0 - A_1 - A_3 \quad (7)$$

$$A_3 = 2A_0 + A_1 - 1 \quad (8)$$

In the present work, both α and S_{max}/σ_o were used as fitting constants, the values of which are shown in table 10.

The threshold ΔK_{th} is approximated by

$$\Delta K_{th} = \Delta K_o \frac{4}{\pi} \arctan(1 - R) \quad (9)$$

where ΔK_o is the threshold stress intensity range at $R = 0$. Also, the fracture toughness K_c for through cracks is defined empirically by

$$\frac{K_c}{K_{Ic}} = 1 + B_k \exp[-(A_k t/t_o)^2] \quad (10)$$

in which t is the thickness and $t_o = 2.5(K_{Ic}/S_y)^2$. These parameters and empirical constants used in establishing the basic crack growth rate curve for this material are listed in table 10. This basic curve showing the crack-growth-rate variation with stress intensity factor range is shown in figure 4. The quality of the curve-fit is evident from this figure where only the data from standard specimens is included. The basic curve is then plotted in comparison with the measured values of crack growth rates for the various part-through-cracked specimens. For each specimen type except the round bars, both the da/dN and dc/dN are shown. Figures 5 through 24 show these plots. These plots also indicate the stress ratio R used for each data set.

Another measure of the validity of using the standard crack growth rate data for life prediction was obtained by comparing the total number of cycles to grow to the final crack size. Crack growth predictions using the material parameters for the base curve were made for all the specimens and compared with the actual measured total growth life. The results are summarized in figures 25 and 26. The results are also shown in tables 11 to 16 in detail. Whenever applicable, growth predictions for both the a -tip and the c -tip are obtained and listed. It is observed that, in most cases, the total cycles for both the tips are about the same, thus validating the two-dimensional growth model. The average ratio of

predicted cycles to experimentally measured cycles for all crack cases, with the exception of the corner crack from a hole under bending, ranged from 0.89 to 1.34. For the cited exceptions, as per the initial calculations, the ratio ranged on an average between 2.07 and 3.5. This was believed to be owing to the inaccuracy in the stress intensity solution for the particular crack case. The equations describing the stress intensity were derived by Newman and Raju[6] and were obtained for a particular ratio of hole diameter to plate thickness(D/t). This solution did not account for the stress concentration affecting the crack at low ratios of hole diameter to plate thickness. Hence, this stress intensity solution for crack case CC02 in bending was modified to include the effect of stress concentration based on a solution by Reissner[7]. A plot of the variation of stress concentration factor with D/t and position of the crack tip is shown in figure 27. The following equation taken from [7] describes the variation of the bending stress concentration factor with the radial coordinate r , hole radius b , and the ratio D/t .

$$K_b = -(1+\nu)A_o - (1-\nu)F_o r^{-2} - 2(1-\nu)E_2 + B_2 r^{-2} - 6(1-\nu)F_2 r^{-4} - \frac{12B_2}{r^2 \xi^2} - C_2 \left[\frac{12K_2(\xi)}{\xi^2} + \frac{4K_1(\xi)}{\xi} \right] \quad (11)$$

where

$$\begin{aligned} \mu &= b\sqrt{10}/t & \xi &= r\sqrt{10}/t \\ A_o &= -1/2(1+\nu) & F_o &= -b^2/2(1-\nu) \\ E_2 &= -1/4(1-\nu) & B_2 &= 2b^2 K_2(\mu)/[(1+\nu)K_2(\mu) + 2K_o(\mu)] \\ C_2 &= -2/[(1+\nu)K_2(\mu) + 2K_o(\mu)] \\ F_2 &= b^4[(1-3\nu)\mu K_2(\mu) + 16K_1(\mu) + 2\mu K_o(\mu)]/12\mu(1-\nu)[(1+\nu)K_2(\mu) + K_o(\mu)] \end{aligned}$$

Also, K_n is the modified Bessel function of order n , and ν is the Poisson's ratio. For the a -tip, the radial coordinate $r = D/2$ was used; and, for the c -tip, the value $r = D/2 + c$ was used to obtain the stress concentration factor.

An empirical factor, which partially takes the finite width into account, was determined so that life predictions match with experimental values on an average basis. The variation of the empirical factor with D/t is shown in figure 28. This factor, C_f , was approximated by

$$C_f = 0.637 - \frac{0.24(D/t)}{\sqrt{19.51 + (D/t)^2}} \quad (12)$$

where an asymptotic value of 0.4 was assumed for large D/t values. It was found that the growth of the a -tip and c -tip matched quite well after the correction due to the bending stress concentration at the hole was introduced in the stress intensity solution. The corrected stress intensity factor was obtained by multiplying the existing solution[6] by the factors K_b and C_f . Once the corrections were included, the average ratio of predicted to test life for this crack case ranged from 0.71 to 1.09.

Discussion

Each of the tables showing fracture toughness or crack growth lives gives all the geometrical information, the nominal and net-section stress levels, and the toughness or total cycle values for each specimen and loading type. The net-section stress is normalized with respect to the yield stress and includes bending stresses induced even under nominally tensile loads. Consider the fracture toughness values first. In the case of a surface crack in a rectangular bar under tensile loading, table 4 shows the data for a number of different thicknesses. The average values of fracture toughness show a trend of reducing toughness with reducing thickness. The toughness values are plotted in relation to the crack depth parameter aF^2 where a is the crack depth and F is the correction factor for the stress intensity factor (as in $K_{Ie} = S_o F \sqrt{\pi a}$). In order to study the effect of the stress level on failure, the normalized stress is also plotted in relation to the factor aF^2 following Newman[8]. Figures 29 and 30 show these two plots. The trends in these plots indicate that the two-parameter approach of Newman[8] may be applicable for this material. This also indicates that crack size and stress level affect the apparent toughness value rather than thickness, since data from specimens of various thicknesses fall along a line. From table 4, it may be observed that most specimens have net-section yielding, and if $K_{Ie}(a)$ were about the same as K_{Ic} , the corresponding net-section stress level at failure would be well below yield. This implies that the net-section yielding possibly contributed to higher toughness values. In order to determine the K_{Ie} value at lower net-section stress levels at failure, larger specimens would be required which were not available during the present investigation.

Referring to the last part of table 4 and table 9, the results of fracture toughness under bending load show high values of toughness at the c -tip. This is because the maximum bending stress occurs at the c -tip where the constraint may be closer to plane stress. In contrast, at the a -tip, the constraint is closer to plane strain resulting in lower toughness. This trend is also found in other crack cases such as the surface crack in round specimens and threaded round bars. The high values of failure stresses for the case of bending loading in table 4 are a result of elastic calculations. In reality, the stresses will be obviously bounded by the yield stress.

From table 5 it is seen that higher failure stresses lead to lower fracture toughness, again in conformity with Newman's two-parameter concept. For some of the specimens in this category, the crack depths were more than the specimen radius, thus exceeding the geometric limits of accuracy of the stress intensity solution. The toughness values from these specimens as a result are found to be lower than the others.

As described in the previous section, the stress intensity solution for the corner-cracked plates in bending (table 9) has been empirically corrected based on matching the predicted

and measured final lives under constant-amplitude loading. The validity of this solution will be further evaluated in the future by using either the three-dimensional finite element or the boundary force method.

In all cases, the test results show that the calculated toughness values for the part-through cracks are higher than the plane-strain values from C(T) specimens. The corner-cracked specimens with open and pin-loaded holes show especially high values of toughness. This is believed to be owing to the high stress gradients near the intersection of crack tip with the hole boundary where plane-stress elastic constraint probably exists.

Looking at the results of crack growth cycle predictions in tables 11 to 16, it is clear that the predictions are in general very good in an average sense. Some scatter does exist among the results for individual specimens. In the case of SC01, the specimens for which the predictions are less than the others in the group are seen to have high levels of stress, closer to the yield strength, thus indicating that the linear elastic approach used here is probably not adequate for these cases. In most specimens, the nominal stress levels were well below the yield strength. Since all the life predictions were based on using the curve fit parameters from standard test specimens, it is evident that for the purpose of fatigue crack growth predictions, use of the data from standard through-cracked specimens is very satisfactory and that the crack-growth predictions using NASA/FLAGRO are accurate for the crack cases studied.

Comparisons of the measured crack growth rates da/dN and dc/dN with the base curve in figures 5 to 24 further confirm the above conclusion because the data fall close to the base curve in almost all cases.

Conclusions

Fatigue crack growth rates from standard specimens can be used with reasonable accuracy in the case of surface and corner cracks, but the fracture toughness values from standard specimens are too conservative for the surface- and corner-cracked cases. A more rigorous stress intensity solution for the corner-cracked specimen with an open hole and loaded in bending needs to be developed to further validate the empirical solution developed herein. The NASA/FLAGRO computer program generally gives accurate results for crack growth prediction of surface and corner cracks if accurate crack-growth-rate material properties are supplied.

References

1. W. G. Reuter, "Relationship Between K_{Ic} (E 399), K_{crit} (Surface Cracks), and Predictions of Structural Integrity," in *Advances in Fracture Research*, eds. K. Salama *et al.*, Proceedings of the Seventh International Conference on Fracture, ICF7, Houston, Texas, March 1989, Pergamon Press, pp. 2595–2602.
2. R. G. Forman and J. A. Henkener, "An Evaluation of the Fatigue Crack Growth and Fracture Toughness Properties of Beryllium-Copper (Be-Cu) Alloy CDA 172," NASA Technical Memorandum 102166, 1990.
3. S. Kalluri and J. Telesman, "Characterization of Fatigue Crack Initiation and Propagation in Ti-6Al-4V With Electrical Potential Drop Technique," NASA Technical Memorandum 100877, July 1988.
4. Fatigue Crack Growth Computer Program "NASA/FLAGRO," Users' Manual, JSC-22267, NASA Lyndon B. Johnson Space Center, March 1989.
5. J. C. Newman Jr., "A Crack Opening Stress Equation for Fatigue Crack Growth," International Journal of Fracture, vol. 24, 1984, pp. R131-R135.
6. J. C. Newman Jr. and I. S. Raju, "Stress Intensity Factor Equations for Cracks in Three-Dimensional Finite Bodies Subjected to Tension and Bending Loads," NASA Technical Memorandum 85793, 1984.
7. E. Reissner, "The Effect of Transverse Shear Deformation on the Bending of Elastic Plates," Journal of Applied Mechanics, June 1945, pp. A-69–A-77.
8. J. C. Newman, Jr., "Fracture Analysis of Surface- and Through-cracked Sheets and Plates," Engineering Fracture Mechanics, vol. 5, 1973, pp. 667–689.

Table 1.- Tensile Test Data for Ti-6Al-4V

Spec. No.	Thickness t in.	Width W in.	Area A sq. in.	Failure Load P_{cr} kip	Yield Stress S_y ksi	Ultimate Stress S_u ksi
1	.099	0.500	0.0495	7350	137.4	148.5
2	.099	0.500	0.0491	7279	138.5	148.2
3	.100	0.496	0.0496	7279	136.7	146.8
Average					137.5	147.8

Table 2.- A Typical Heat-tint Schedule

Temperature ° F	Soaking Time Hours
1000	2.0
1000	1.0
900	2.0
800	2.0
700	2.0
600	2.0
400	2.0

This schedule was used for the corner crack from open hole in bending.

Table 3.- Plane-Strain Fracture Toughness from C(T) Specimens

Spec. No.	Orient.	Width W in.	Thickness t in.	Hole Dia. D in.	Crack Depth a in.	Failure Stress S_{cr} ksi	Net-section Stress Ratio S_{net}/S_y	Fracture Toughness K_{Ic} ksi $\sqrt{in.}$
T-2	L-T	2.00	0.9	0.5	1.264	8.89	0.470	49.0
T-3	L-T	2.00	0.9	0.5	1.204	10.44	0.462	50.8
Average								49.9
T-4	T-L	2.00	0.9	0.5	1.017	11.76	0.322	41.2
T-5	T-L	2.00	0.9	0.5	1.029	12.00	0.338	43.0
T-6	T-L	2.00	0.9	0.5	1.003	11.88	0.314	40.8
Average								41.7

Table 4.- Fracture Toughness from Surface-Cracked Rectangular Specimens

Spec. No.	Thick-ness t in.	Width W in.	Crack Depth a in.	Crack Length c in.	Tensile Loading			Fracture Toughness	
					Aspect Ratio a/c	Failure Stress S_{cr} ksi	Net-section Stress Ratio S_{net}/S_y	a-tip $K_{Ic}(a)$ ksi $\sqrt{in.}$	c-tip $K_{Ic}(c)$ ksi $\sqrt{in.}$
TA-3	.05	1.8	0.0434	0.0718	0.60	128.4	1.04	49.5	52.3
TA-4	.05	1.8	0.0420	0.0654	0.64	133.2	1.07	48.2	51.9
TA-7	.05	1.8	0.0400	0.0635	0.63	134.4	1.08	47.7	49.8
TA-8	.05	1.8	0.0280	0.0594	0.47	138.7	1.09	44.6	37.0
TA-9	.05	1.8	0.0441	0.0657	0.67	138.7	1.11	50.3	56.3
Average								48.1	49.5
TB-1	.15	1.8	0.1193	0.1380	0.86	126.6	1.14	62.8	77.2
TB-3	.15	1.8	0.1076	0.1185	0.91	126.9	1.11	56.8	69.3
TB-4	.15	1.8	0.0937	0.1049	0.89	130.8	1.11	54.3	63.5
TB-5	.15	1.8	0.0707	0.0857	0.82	137.6	1.11	50.7	54.2
TB-6	.15	1.8	0.0877	0.0981	0.89	137.6	1.15	54.8	63.2
TB-7	.15	1.8	0.0870	0.0958	0.89	138.5	1.15	54.4	63.1
TB-8	.15	1.8	0.0888	0.0969	0.92	122.4	1.02	48.3	56.6
TB-9	.15	1.8	0.0867	0.0803	0.93	135.6	1.10	50.0	57.7
TB-10	.15	1.8	0.1135	0.1320	0.86	106.7	0.95	51.5	62.1
TB-11	.15	1.8	0.1162	0.1327	0.87	104.2	0.93	50.4	61.7
Average								53.4	62.9
TC-1	.245	1.80	0.2028	0.2341	0.87	101.9	1.13	67.6	84.4
TC-3	.252	1.56	0.1443	0.1465	0.98	124.5	1.15	59.8	72.2
TC-4	.251	1.56	0.1547	0.1667	0.93	106.0	1.03	55.7	66.2
TC-5	.251	1.61	0.1382	0.1563	0.88	110.5	1.04	55.8	63.3
TC-6	.251	1.53	0.1461	0.1577	0.93	100.5	0.95	51.0	59.8
TC-7	.250	1.60	0.1448	0.1523	0.95	113.8	1.07	56.3	66.8
TC-8	.251	1.57	0.1467	0.1592	0.92	108.3	1.03	55.2	64.7
Average								57.3	68.2

Table 4.- Concluded

<u>Tensile Loading(contd.)</u>									
Spec. No.	Thick-ness t in.	Width W in.	Crack Depth a in.	Crack Length c in.	Aspect Ratio a/c	Failure Stress S_{cr} ksi	Net-section Stress Ratio S_{net}/S_y	Fracture Toughness	
								a-tip $K_{Ie}(a)$ ksi $\sqrt{in.}$	c-tip $K_{Ie}(c)$ ksi $\sqrt{in.}$
14	0.40	2.80	0.106	0.097	1.09	149.0	1.14	54.8	64.3
1	0.40	2.80	0.149	0.236	0.63	138.2	1.18	83.6	76.4
2	0.40	2.80	0.140	0.229	0.61	127.2	1.08	75.1	67.2
3	0.40	2.80	0.162	0.256	0.63	115.5	1.01	73.7	67.9
4	0.40	2.80	0.174	0.271	0.64	125.3	1.13	83.0	77.5
20	0.40	2.80	0.202	0.369	0.58	101.7	1.03	81.7	71.9
11	0.40	2.80	0.178	0.293	0.61	100.4	0.92	69.6	63.4
12	0.40	2.80	0.183	0.280	0.65	115.1	1.05	78.2	74.1
13	0.39	2.78	0.216	0.417	0.52	113.6	1.24	99.8	86.8
Average								77.7	72.2

<u>Bending Loading</u>									
Spec. No.	Thick-ness t in.	Width W in.	Crack Depth a in.	Crack Length c in.	Aspect Ratio a/c	Failure Stress S_{cr} ksi	Net-section Stress Ratio S_{net}/S_y	Fracture Toughness	
								a-tip $K_{Ie}(a)$ ksi $\sqrt{in.}$	c-tip $K_{Ie}(c)$ ksi $\sqrt{in.}$
8	0.40	2.80	0.116	0.137	0.85	222.0	1.72	61.4	90.5
9	0.40	2.80	0.125	0.164	0.76	223.0	1.76	65.0	95.0
10	0.40	2.80	0.125	0.161	0.78	218.0	1.72	63.1	92.7
15	0.40	2.80	0.187	0.219	0.85	84.4	0.71	37.7	86.2
18	0.40	2.80	0.230	0.259	0.89	214.2	1.94	33.0	120.0
19	0.41	2.80	0.148	0.230	0.64	170.3	1.41	52.3	79.4
Average								52.1	94.0

Table 5.- Fracture Toughness from Surface-Cracked Round Specimens

<u>Tensile Loading</u>					
Spec. No.	Diameter	Crack Depth	Failure Stress	Net-section Stress Ratio	Fracture Toughness
	D	a	S_{cr}	S_{net}/S_y	$K_{Ic}(a)$
	in.	in.	ksi		ksi $\sqrt{in.}$
RD 1	0.90	0.400	47.2	1.35	73.9
RD 2	0.90	0.394	47.1	1.29	71.5
RD 3	0.90	0.390	47.0	1.25	70.1
RD 4	0.90	0.680	6.9	2.00	51.9
RD 5	0.90	0.582	12.5	1.38	48.7
RD 6	0.90	0.580	14.5	1.57	55.8
RD 7	0.90	0.538	18.4	1.43	56.2
Average					61.2

<u>Bending Loading</u>					
Spec. No.	Diameter	Crack Depth	Failure Stress	Net-section Stress Ratio	Fracture Toughness
	D	a	S_{cr}	S_{net}/S_y	$K_{Ic}(a)$
	in.	in.	ksi		ksi $\sqrt{in.}$
RD 8	0.90	0.520	30.7	0.76	41.0
RD 9	0.90	0.343	80.0	0.74	58.5
RD 10	0.90	0.349	70.2	0.66	52.3
RD 11	0.90	0.175	139.1	0.84	62.6
RD 12	0.90	0.550	31.4	0.93	47.0
Average					52.3

Table 6.- Fracture Toughness from Surface-Cracked Threaded Round Specimens

<u>Tensile Loading</u>					
Spec. No.	Diameter	Crack Depth	Failure Stress	Net-section Stress Ratio	Fracture Toughness
	D in.	a in.	S_{cr} ksi	S_{net}/S_y	$K_{Ic}(a)$ ksi $\sqrt{in.}$
TH 1	0.78	0.245	79.2	1.10	69.6
TH 2	0.78	0.206	91.0	1.05	65.8
TH 3	0.78	0.263	83.7	1.29	79.9
TH 4	0.78	0.303	62.0	1.25	72.3
Average					71.9

<u>Bending Loading</u>					
Spec. No.	Diameter	Crack Depth	Failure Stress	Net-section Stress Ratio	Fracture Toughness
	D in.	a in.	S_{cr} ksi	S_{net}/S_y	$K_{Ic}(a)$ ksi $\sqrt{in.}$
TH 1B	0.78	0.232	107.3	0.77	58.8
TH 2B	0.78	0.236	115.9	0.84	64.3
TH 4B	0.78	0.302	67.1	0.63	46.3
TH 5B	0.78	0.295	93.9	0.86	63.4
Average					58.2

Table 7.- Fracture Toughness from Corner-Cracked Rectangular Specimens

Spec. No.	Thick-ness t in.	Width W in.	<u>Tensile Loading</u>				Fracture Toughness		
			Crack Depth a in.	Crack Length c in.	Aspect Ratio a/c	Failure Stress S_{cr} ksi	Net-section Stress Ratio S_{net}/S_y	a-tip $K_{Ic}(a)$ ksi $\sqrt{in.}$	c-tip $K_{Ic}(c)$ ksi $\sqrt{in.}$
1 E	0.45	0.90	0.338	0.312	1.08	61.5	0.98	62.7	66.5
2 E	0.45	0.90	0.242	0.203	1.19	73.4	0.79	48.4	53.4
4 C	0.45	0.90	0.170	0.300	0.57	94.6	1.02	71.1	57.3
5 C	0.45	0.90	0.261	0.236	1.11	71.2	0.82	53.1	56.9
6 C	0.45	0.90	0.284	0.213	1.33	95.0	1.08	66.9	77.0
7 C	0.45	0.90	0.230	0.344	0.67	60.2	0.76	55.4	48.5
Average								59.6	59.9

Table 8.- Fracture Toughness from Corner-Cracked Rectangular Specimens (Open Hole)

Spec. No.	Thick-ness t in.	Width W in.	Hole Dia. D in.	Crack Depth a in.	Crack Length c in.	Aspect Ratio a/c	Tensile Loading		Fracture Toughness	
							Failure Stress S_{cr} ksi	Net-section Stress Ratio S_{net}/S_y	a-tip $K_{Ic}(a)$ ksi $\sqrt{in.}$	c-tip $K_{Ic}(c)$ ksi $\sqrt{in.}$
1 A	0.483	2.90	0.50	0.379	0.272	1.39	64.3	0.66	83.2	64.3
2 A	0.492	2.90	0.50	0.378	0.274	1.38	62.7	0.65	81.3	77.3
3 A	0.500	2.90	0.50	0.416	0.261	1.59	81.2	0.83	102.9	104.8
4 A	0.497	2.90	0.50	0.209	0.192	1.09	55.5	0.53	64.9	51.6
5 A	0.491	2.89	0.50	0.357	0.234	1.53	89.6	0.90	110.5	107.9
6 A	0.500	2.90	0.50	0.262	0.221	1.19	83.1	0.82	101.3	85.0
7 A	0.497	2.91	0.50	0.457	0.310	1.47	78.2	0.83	104.7	107.0
8 A	0.492	2.90	0.50	0.394	0.309	1.28	82.0	0.87	110.5	103.5
9 A	0.491	2.91	0.50	0.417	0.338	1.23	83.4	0.90	115.6	109.3
10 A	0.490	2.91	0.50	0.300	0.229	1.31	96.6	0.96	119.0	106.4
Average									99.4	91.7

Table 9.- Fracture Toughness from Corner-Cracked Rectangular Specimens (Open Hole)

Spec. No.	Thick-ness t in.	Width W in.	Hole Dia. D in.	<u>Bending Loading</u>			Failure Stress S_{cr} ksi	Net-section Stress Ratio S_{net}/S_y	Fracture Toughness	
				Crack Depth a in.	Crack Length c in.	Aspect Ratio a/c			a-tip $K_{Ic}(a)$ ksi $\sqrt{in.}$	c-tip $K_{Ic}(c)$ ksi $\sqrt{in.}$
B-2	0.450	2.00	0.50	0.2152	0.3216	0.67	115.2	1.01	52.7	87.2
B-3	0.450	2.00	0.50	0.1561	0.2173	0.72	115.9	0.94	64.2	77.7
B-4	0.450	2.00	0.50	0.1990	0.3043	0.65	120.4	1.04	59.9	86.9
B-5	0.450	2.00	0.50	0.2197	0.3479	0.63	103.0	0.93	48.0	78.3
B-6	0.450	2.00	0.50	0.2358	0.2740	0.86	104.5	0.89	36.4	87.3
B-7	0.450	2.00	0.50	0.2053	0.3182	0.65	116.7	1.02	57.1	85.4
B-8	0.450	2.00	0.50	0.2295	0.3686	0.62	110.4	1.01	49.6	86.4
C-1	0.375	3.00	0.75	0.1796	0.3158	0.57	133.7	1.09	63.5	95.9
C-2	0.375	3.00	0.75	0.1250	0.1670	0.75	112.0	0.86	58.6	75.6
C-3	0.375	3.00	0.75	0.1423	0.1952	0.73	103.5	0.80	51.2	72.1
C-4	0.375	3.00	0.75	0.1817	0.3068	0.59	144.0	1.17	66.0	105.0
Average									55.2	85.3

Table 10.- Basic Crack Growth Constants used for Life Prediction in Ti-6Al-4V

Constant	Value
$C:$	0.242E-08
$n:$	3.007
$p:$	0.25
$q:$	0.75
$\Delta K_0:$	3.5
$K_{Ic}:$	50.0
$K_{Ic}:$	75.0
$A_k:$	0.75
$B_k:$	1.00
$\alpha:$	2.0
$S_{max}/\sigma_0:$	0.3

Table 11.- Life Prediction for SC01

<u>Surface Crack in Rectangular Bar under Tension, W = 2.8, t = 0.4, R = 0.05</u>										
Spec. No.	Max. Stress	Net stress S_{net}/S_y	a_i in.	a_f in.	c_i in.	c_f in.	a_i/c_i	Life N_e	a-tip N_t/N_e	c-tip N_t/N_e
14	89.22	0.68	.0560	.1060	.046	.0970	1.22	2340	1.00	0.95
15	71.48	0.62	.0385	.1871	.0320	.2194	1.20	10599	1.03	1.05
16	53.49	0.47	.0410	.2074	.0400	.2203	1.03	19212	1.31	1.32
18	88.88	0.82	.1225	.2296	.1122	.2590	1.09	1256	0.75	0.79
Average									1.02	1.03
<u>Surface Crack in Rectangular Bar under 3-pt Bending, W = 2.8, t = 0.4, R = 0.05</u>										
Spec. No.	Max. Stress	Net stress S_{net}/S_y	a_i in.	a_f in.	c_i in.	c_f in.	a_i/c_i	Life N_e	a-tip N_t/N_e	c-tip N_t/N_e
1	40.58	0.34	.053	.149	.0595	.2355	0.89	50230	1.68	1.69
2	46.82	0.39	.040	.140	.0460	.2285	0.87	45871	1.37	1.43
3	67.29	0.57	.037	.162	.0440	.2560	0.84	16284	1.38	1.35
4	79.02	0.69	.070	.174	.0575	.2705	1.22	8509	1.20	1.11
6	86.46	0.74	.055	.168	.0525	.2610	1.05	7360	1.11	1.05
20	100.92	0.97	.082	.202	.0925	.3690	0.89	3786	1.02	0.93
Average									1.29	1.26
<u>Surface Crack in Rectangular Bar under Cantilever Bending, W = 2.8, t = 0.4, R = 0.05</u>										
Spec. No.	Max. Stress	Net stress S_{net}/S_y	a_i in.	a_f in.	c_i in.	c_f in.	a_i/c_i	Life N_e	a-tip N_t/N_e	c-tip N_t/N_e
7	64.57	0.50	.029	.105	.0345	.1425	0.84	21344	1.04	1.07
8	79.56	0.62	.056	.116	.0545	.1365	1.03	7494	0.94	0.83
9	94.69	0.75	.042	.125	.0440	.1635	0.95	4863	1.12	1.07
10	106.35	0.84	.047	.125	.0490	.1605	0.96	3412	0.96	0.90
11	125.05	1.11	.049	.178	.0520	.2930	0.94	3150	0.76	0.72
12	138.44	1.22	.051	.183	.0550	.2800	0.93	2400	0.66	0.60
13	127.58	1.32	.167	.216	.2210	.4170	0.76	1161	0.52	0.40
19	57.82	0.48	.047	.148	.0475	.2300	0.99	28771	1.07	1.07
Average									0.88	0.83

Table 12.- Life Prediction for SC07

Surface Crack in Round Bar under Tension, D = 0.9, R = 0.1

Spec. No.	Max. Stress	Net stress S_{net}/S_y	a_i in.	a_f in.	N_e	a -tip N_i/N_e
RD-1 T	23.57	0.20	.0421	.1317	200014	1.39
RD-2 T	18.82	0.26	.0637	.2780	380855	1.11
RD-3 T	15.64	0.16	.0657	.2030	787332	0.89
RD-4T	6.92	2.00	.5404	.6800	2493	2.21 [†]
RD-5 T	12.55	1.38	.3695	.5820	11586	1.32
RD-6 T	11.01	1.19	.3670	.5800	22898	1.08
RD-7 T	11.00	0.86	.3650	.5380	19626	1.27
Average						1.18

[†]Accuracy of the K-solution suspect for $a/D > 0.5$, not included in the average.

Surface Crack in Round Bar under Bending, D = 0.9, R = 0.1

Spec. No.	Max. Stress	Net stress S_{net}/S_y	a_i in.	a_f in.	N_e	a -tip N_i/N_e
RD-8 B	26.20	0.65	.0791	.5200	200448	1.18
RD-9 B	20.96	0.19	.0524	.3430	799514	0.87
RD-10B	34.93	0.33	.0592	.3490	97541	1.19
RD-11B	43.81	0.27	.0588	.1753	38094	1.12
RD-12B	20.68	0.61	.0772	.5500	806505	0.66
Average						1.00

Table 13.- Life Prediction for SC08

Surface Crack in Threaded Round Bar under Tension, $2r = 0.78$, $R = 0.1$

Spec. No.	Max. Stress	Net stress S_{net}/S_y	a_i in.	a_f in.	N_e	a -tip N_i/N_e
TH-1	41.86	0.58	.1740	.2450	5149	0.50
TH-2	31.39	0.36	.1187	.2060	19669	1.00
TH-4	41.86	0.39	.0619	.1432	14011	1.66
TH-5	24.78	0.21	.0471	.1050	112917	1.47
Average						1.16

Surface Crack in Threaded Round Bar under Bending, $2r = 0.78$, $R = 0.1$

Spec. No.	Max. Stress	Net stress S_{net}/S_y	a_i in.	a_f in.	N_e	a -tip N_i/N_e
TH-1B	40.24	0.29	.0629	.2321	74622	0.81
TH-2B	32.19	0.23	.0771	.2358	197961	0.51
TH-3B	53.65	1.06	.0663	.4168	34554	0.72
TH-4B	67.10	0.63	.0657	.3015	11439	0.99
TH-5B	93.90	0.86	.0562	.2950	3911	1.02
Average						0.81

Table 14.- Life Prediction for CC01

<u>Corner Crack in Rectangular Bar under Tension, W = 0.9, t = 0.45, R = 0.1</u>										
Spec. No.	Max. Stress	Net stress S_{net}/S_y	a_i in.	a_f in.	c_i in.	c_f in.	a_i/c_i	Life N_e	a-tip N_t/N_e	c-tip N_t/N_e
1-E	49.38	0.78	.0835	.3378	.0796	.3116	1.05	14012	1.24	1.23
2-E	73.42	1.45	.0784	.4297	.0775	.2710	1.01	3709	1.26	1.22
Average									1.25	1.22
<u>Corner Crack in Rectangular Bar under Bending, W = 0.9, t = 0.9, R = 0.05</u>										
Spec. No.	Max. Stress	Net stress S_{net}/S_y	a_i in.	a_f in.	c_i in.	c_f in.	a_i/c_i	Life N_e	a-tip N_t/N_e	c-tip N_t/N_e
1-D	24.66	0.23	.0649	.2203	.0565	.3235	1.15	412909	0.83	0.87
2-D	74.07	0.72	.0681	.2740	.0721	.3420	0.94	11088	0.89	0.83
3-D	41.06	0.39	.0600	.253	.067	.341	0.89	66188	1.11	1.10
Average									0.94	0.93
<u>Corner Crack in Rectangular Bar under Bending, W = 0.9, t = 0.5, R = 0.05</u>										
Spec. No.	Max. Stress	Net stress S_{net}/S_y	a_i in.	a_f in.	c_i in.	c_f in.	a_i/c_i	Life N_e	a-tip N_t/N_e	c-tip N_t/N_e
1-C	49.6	0.52	.0858	.2072	.0864	.3577	0.99	30807	1.24	1.24
2-C	65.8	0.64	.0628	.1988	.0668	.2880	0.94	16087	1.34	1.25
3-C	99.2	1.00	.0599	.2216	.0725	.3075	0.83	3842	1.28	1.13
4-C	32.9	0.32	.0656	.1697	.0790	.2990	0.83	164896	1.11	1.11
Average									1.24	1.18
<u>Corner Crack in Rectangular Bar under Bending, W = 0.9, t = 0.45, R = 0.05</u>										
Spec. No.	Max. Stress	Net stress S_{net}/S_y	a_i in.	a_f in.	c_i in.	c_f in.	a_i/c_i	Life N_e	a-tip N_t/N_e	c-tip N_t/N_e
5-C	32.9	0.32	.0633	.2614	.0586	.2361	1.08	86330	1.44	1.53
6-C	82.3	0.79	.0695	.2836	.0618	.2131	1.12	6665	0.76	0.75
Average									1.10	1.14

Table 15.- Life Prediction for CC02

Corner Crack from a Hole in Rectangular Bar, 3-pt. Bending

Spec. No.	Max. Stress	Net stress S_{net}/S_y	a_i in.	a_f in.	c_i in.	c_f in.	a_i/c_i	Life N_e	a-tip N_t/N_e	c-tip N_t/N_e
<u>W = 2.0, t = 0.45, D = 0.5, S = 8.0, R = 0.05</u>										
1-B	41.47	0.35	.053	.193	.062	.278	0.85	32430	0.49	0.45
2-B	29.64	0.25	.074	.195	.077	.289	0.96	89250	0.51	0.48
3-B	20.72	0.17	.047	.181	.047	.266	1.01	282300	0.51	0.51
4-B	15.62	0.13	.059	.174	.068	.286	0.87	528672	0.58	0.68
5-B	47.23	0.42	.064	.221	.066	.343	0.97	12761	1.04	0.91
6-B	29.59	0.26	.071	.216	.063	.339	1.13	43100	1.36	1.24
Average									0.75	0.71
<u>W = 2.0, t = 0.45, D = 0.5, S = 5.0, R = 0.1</u>										
B-2	22.22	0.19	.1064	.2152	.1038	.3216	1.03	82591	1.58	1.34
B-3	16.67	0.14	.0784	.1561	.0771	.2173	1.02	216691	0.84	0.90
B-4	22.22	0.19	.1155	.1990	.1178	.3043	0.98	67208	1.48	1.41
B-5	55.56	0.50	.1080	.2197	.1196	.3479	0.90	12154	0.52	0.45
B-6	74.07	0.74	.0935	.2358	.1173	.4760	0.80	3363	0.83	0.83
B-7	16.67	0.15	.1000	.2053	.0876	.3182	1.14	327271	0.96	0.90
B-8	74.07	0.68	.0688	.2295	.0727	.3686	0.95	5110	0.58	0.48
Average									0.97	0.90
<u>W = 1.9, t = 0.9, D = 0.375, R = 0.1</u>										
A-2	34.11	0.30	.1875	.3510	.1327	.3642	1.41	25618	0.97	0.66
A-3	19.49	0.16	.1120	.2573	.1150	.2482	0.97	69533	1.31	0.97
A-4	18.52	0.15	.1200	.2343	.0940	.2380	1.28	88074	0.98	0.87
Average									1.09	0.83
<u>W = 3.0, t = 0.375, D = 0.75, R = 0.1</u>										
C-1	17.78	0.15	.0967	.1796	.0995	.3158	0.97	261596	0.90	0.88
C-2	12.44	0.09	.0722	.1250	.0745	.1670	0.97	550164	0.71	0.67
C-3	17.78	0.14	.0775	.1423	.0772	.1952	1.00	134470	1.16	1.03
C-4	17.78	0.15	.0785	.1817	.0763	.3068	1.03	205122	1.35	1.24
Average									1.03	0.96

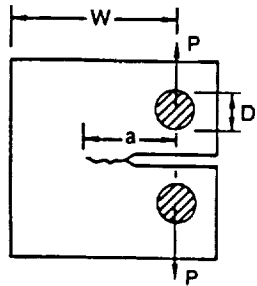
Table 15.- Concluded

Corner Crack from a Hole in Rectangular Bar - Tension, $W = 2.9$, $t = 0.5$, $D = 0.5$, $R = 0.05$

Spec. No.	Max. Stress	Net stress S_{net}/S_y	a_i in.	a_f in.	c_i in.	c_f in.	a_i/c_i	Life N_e	a-tip N_i/N_e	c-tip N_i/N_e
2-A	28.03	0.29	.038	.378	.038	.274	1.00	18713	1.24	1.24
3-A	22.06	0.23	.065	.416	.037	.261	1.76	79045	0.58	0.54
4-A	55.51	0.53	.046	.209	.040	.192	1.15	1762	0.80	0.91
5-A	22.58	0.23	.037	.357	.037	.234	1.00	44384	1.06	1.01
6-A	41.39	0.41	.041	.262	.039	.221	1.05	5862	0.84	0.91
7-A	19.38	0.21	.164	.457	.116	.310	1.41	18957	1.96	1.79
8-A	35.05	0.37	.045	.394	.040	.309	1.13	10505	0.99	1.01
9-A	42.03	0.45	.046	.417	.043	.338	1.07	5357	1.02	1.05
10-A	49.18	0.49	.040	.300	.038	.229	1.05	4769	0.60	0.62
Average									1.01	1.01

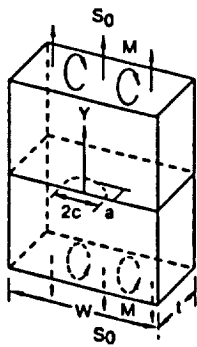
Table 16.- Life Prediction for CC03

<u>Corner Crack from a Hole in Rectangular Bar - Pin Loading</u>										
Spec. No.	Max. Stress	Net stress S_{net}/S_y	a_i in.	a_f in.	c_i in.	c_f in.	a_i/c_i	Life N_e	a-tip N_t/N_e	c-tip N_t/N_e
<u>W = 2.9, t = 0.5, D = 0.5, R = 0.05</u>										
PA-2	48.60	0.08	.0361	.4179	.0334	.2218	1.08	97015	0.91	0.89
PA-3	72.67	0.13	.0410	.3890	.0375	.2220	1.09	21251	1.00	1.03
PA-4	61.27	0.11	.0327	.4310	.0325	.2221	1.00	42356	1.02	0.97
Average									0.98	0.96
<u>W = 1.5, t = 0.5, D = 0.5, R = 0.05</u>										
PC-1	64.10	0.34	.0497	.3628	.0449	.2323	1.11	8131	0.92	0.99
PC-2	40.09	0.21	.0311	.3845	.0298	.2127	1.04	43413	1.05	1.03
PC-3	48.58	0.25	.0362	.3710	.0336	.2168	1.08	20408	1.10	1.11
PC-4	73.00	0.38	.0423	.3480	.0382	.2231	1.11	7624	0.65	0.70
PC-5	89.00	0.47	.0418	.3363	.0394	.2278	1.06	4843	0.47	0.53
Average									0.84	0.87
<u>W = 1.0, t = 0.5, D = 0.5, R = 0.05</u>										
PD-1	41.01	0.65	.0345	.2956	.0332	.2119	1.04	8992	0.95	1.00
PD-2	24.03	0.46	.0343	.3814	.0315	.2176	1.09	35166	1.57	1.56
PD-3	20.27	0.38	.0349	.3830	.0361	.2134	1.00	62362	1.50	1.49
PD-4	48.96	0.80	.0368	.2990	.0347	.2176	1.06	6143	0.72	0.76
PD-5	60.68	0.44	.0370	.3314	.0350	.2536	1.06	3304	0.62	0.62
Average									1.07	1.09
<u>W = 2.9, t = 0.5, D = 0.5, $\phi = 9^\circ$, R = 0.05</u>										
PB-1	60.00	0.10	.0335	.3950	.0341	.2135	1.00	48641	0.89	0.87
PB-2	48.25	0.08	.0348	.4640	.0330	.2079	1.05	92818	1.07	0.90
PB-3	72.79	0.13	.0983	.3947	.0749	.2192	1.31	14205	1.06	1.08
PB-5	73.09	0.13	.0468	.4860	.0400	.2270	1.17	22293	1.08	0.95
Average									1.03	0.95



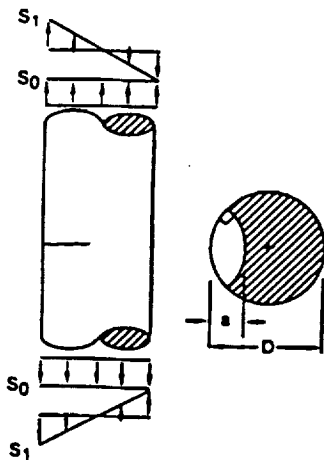
L-T ori.: $K_{Ic} = 49, 51$ Avg. $\rightarrow 50$

T-L ori.: $K_{Ic} = 41, 43, 41$ Avg. $\rightarrow 42$



Tension: $K_{Ic}(a) = 55, 84, 75, 74, 83, 82, 70, 78,$
100 Avg. $\rightarrow 78$

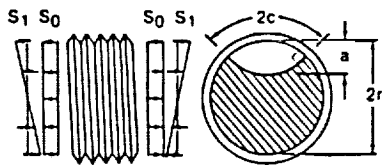
Bending: $K_{Ic}(c) = 91, 95, 93, 86, 120, 79$ Avg. $\rightarrow 94$



Tension: $K_{Ic} = 74, 72, 70, 52, 49, 56, 56$ Avg. $\rightarrow 61$

Bending: $K_{Ic} = 41, 59, 52, 63, 47$ Avg. $\rightarrow 52$

Figure 1.- Summary of fracture toughness results.

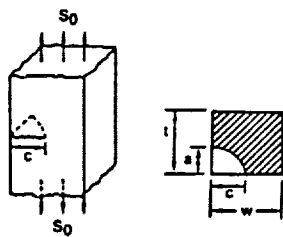


Tension: $K_{Ic} = 70, 66, 80, 72$

Avg. → 72

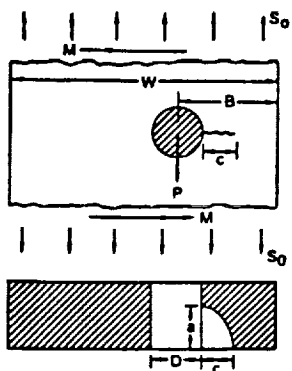
Bending: $K_{Ic} = 59, 64, 46, 63$

Avg. → 58



Tension: $K_{Ic} = 66, 53, 71, 57, 77, 55$

Avg. → 63



Tension: $K_{Ic}(a) = 83, 81, 103, 65, 111,$

102, 105, 111, 116, 119

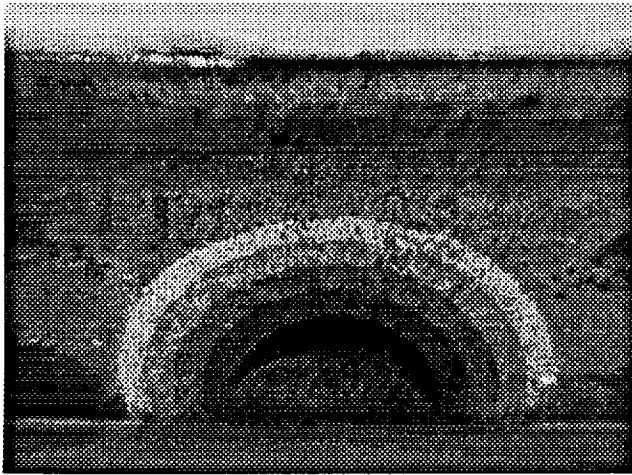
Avg. → 99

Bending: $K_{Ic}(c) = 87, 78, 87, 78, 87,$

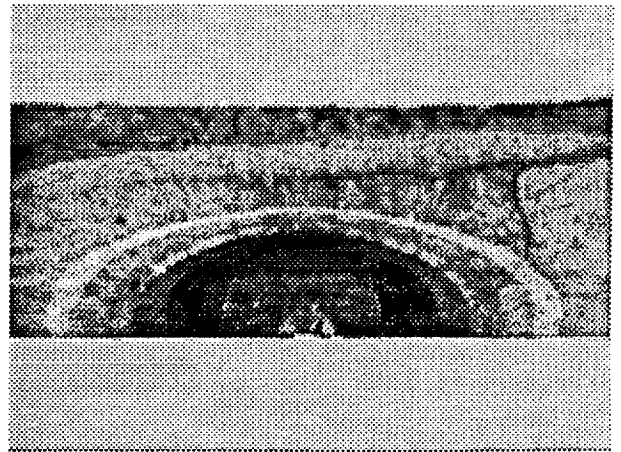
85, 86, 96, 76, 72, 105

Avg. → 85

Figure 2.- Summary of fracture toughness results.

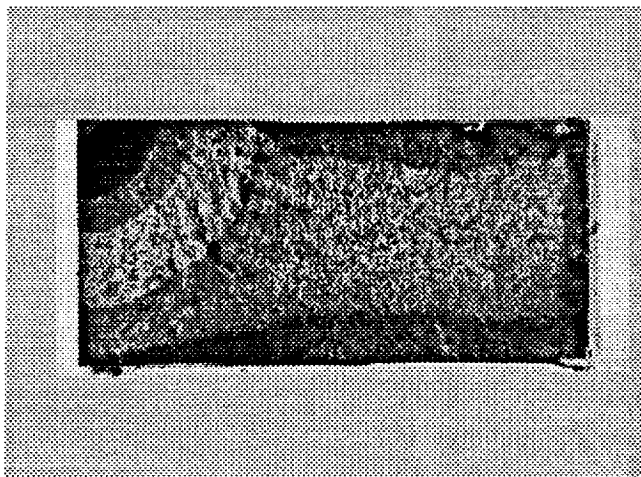


Surface Crack - Tension

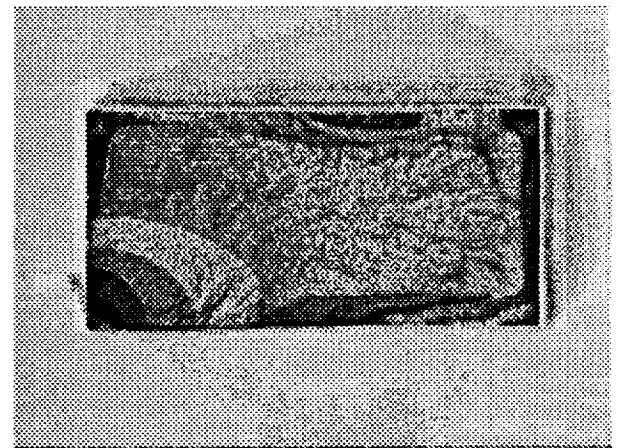


Surface Crack - Bending

ORIGINAL PAGE IS
OF POOR QUALITY



Corner Crack - Tension



Corner Crack - Bending

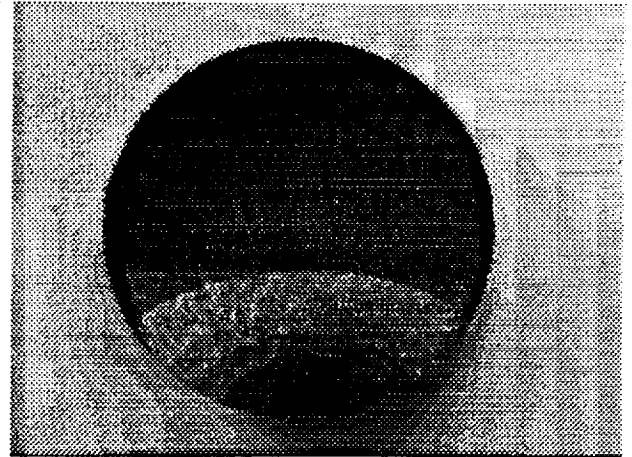
(a) SC01 and CC01

Figure 3.- Crack surfaces showing heat-tint marks.

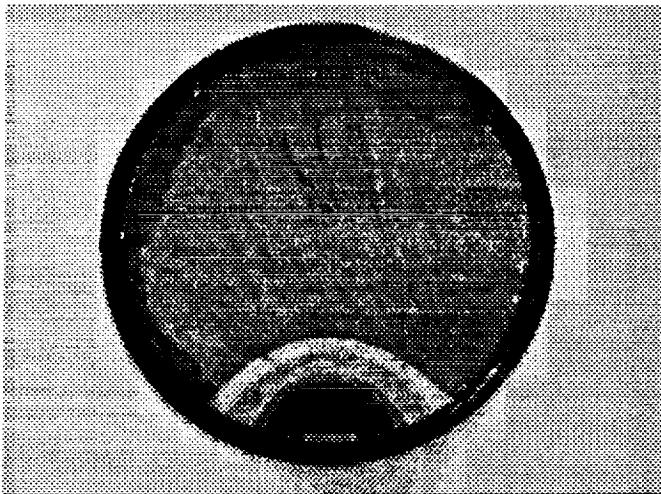
**ORIGINAL PAGE IS
OF POOR QUALITY**



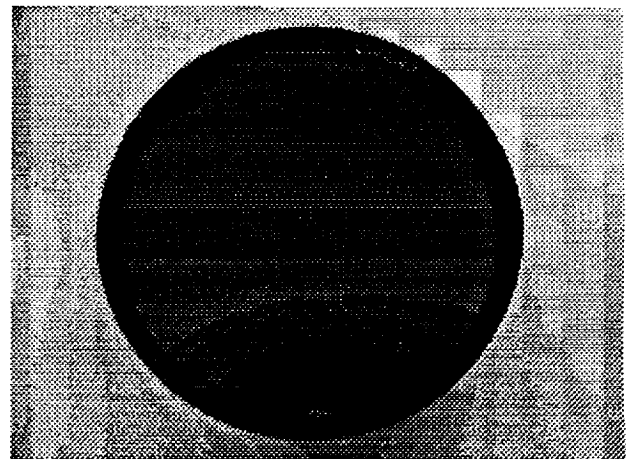
Round Bar - Tension



Round Bar - Bending



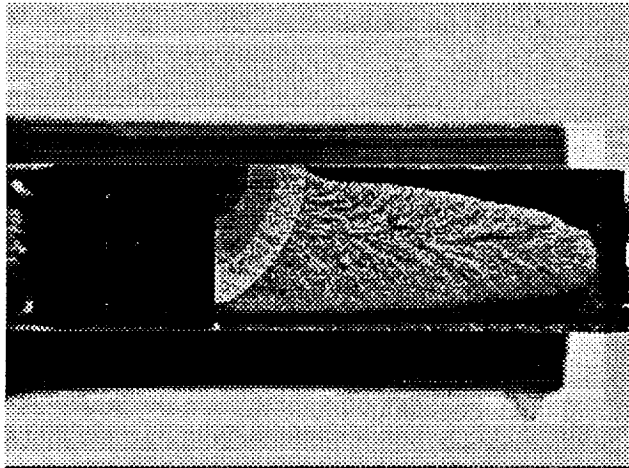
Threaded Round Bar - Tension



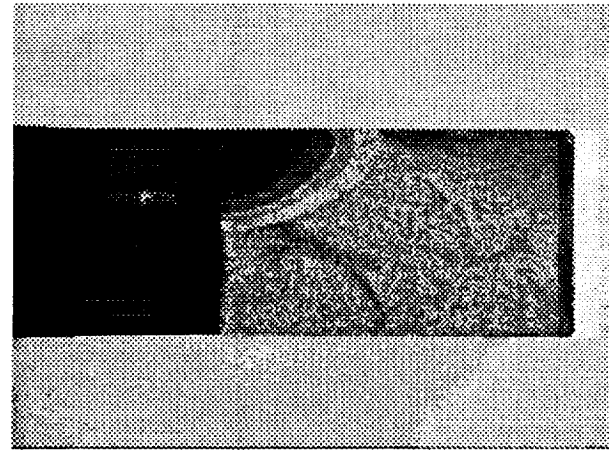
Threaded Round Bar - Bending

(b) SC07 and SC08

Figure 3.- Continued.

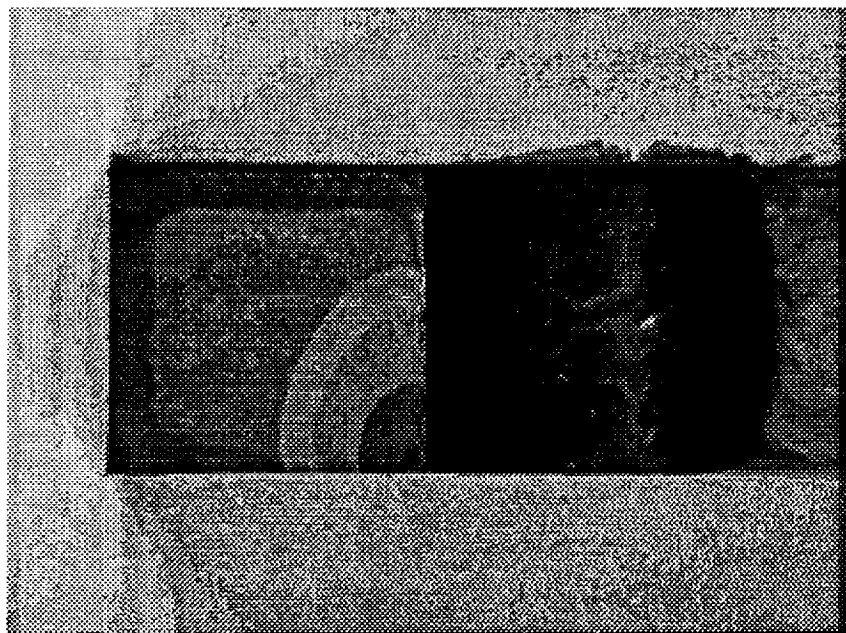


Corner Crack from Hole - Tension



Corner Crack from Hole - Bending

ORIGINAL PAGE IS
OF POOR QUALITY



Corner Crack - Pin Loading

(c) CC02 and CC03

Figure 3.- Concluded.

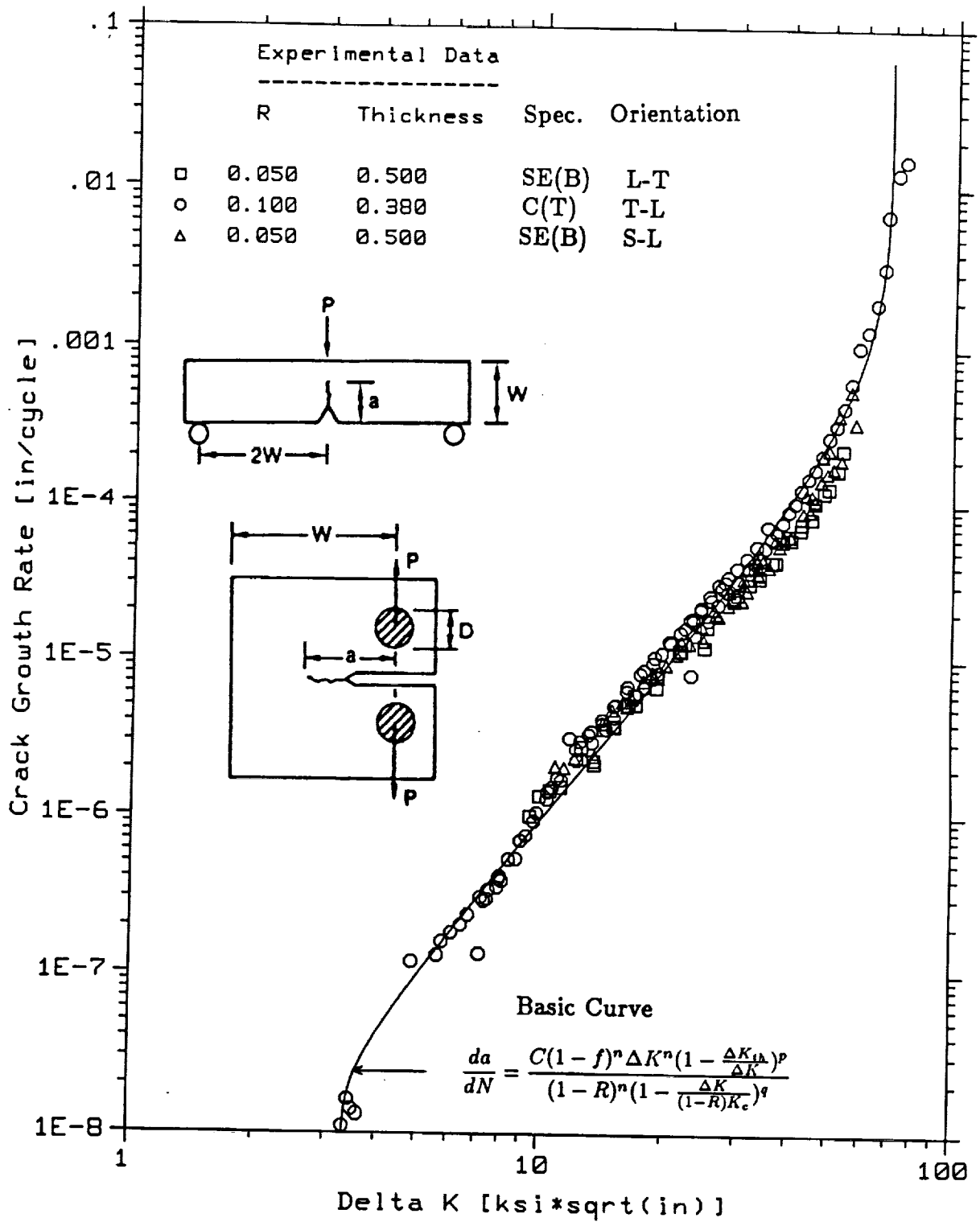


Figure 4.- Base curve fit of fatigue crack growth rates, data from standard specimens.

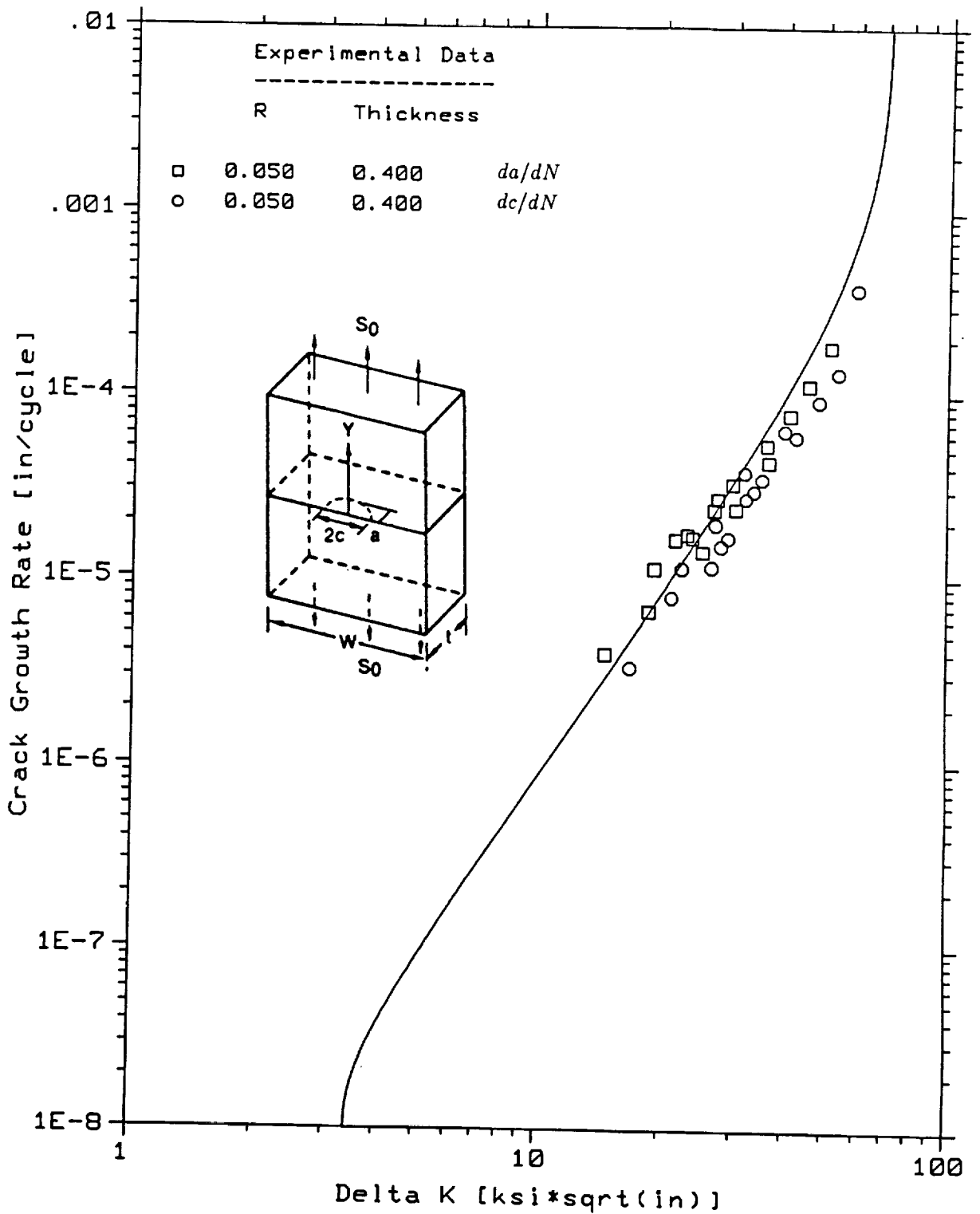


Figure 5.- Comparison of fatigue crack growth rates, surface crack in rectangular bar - tension.

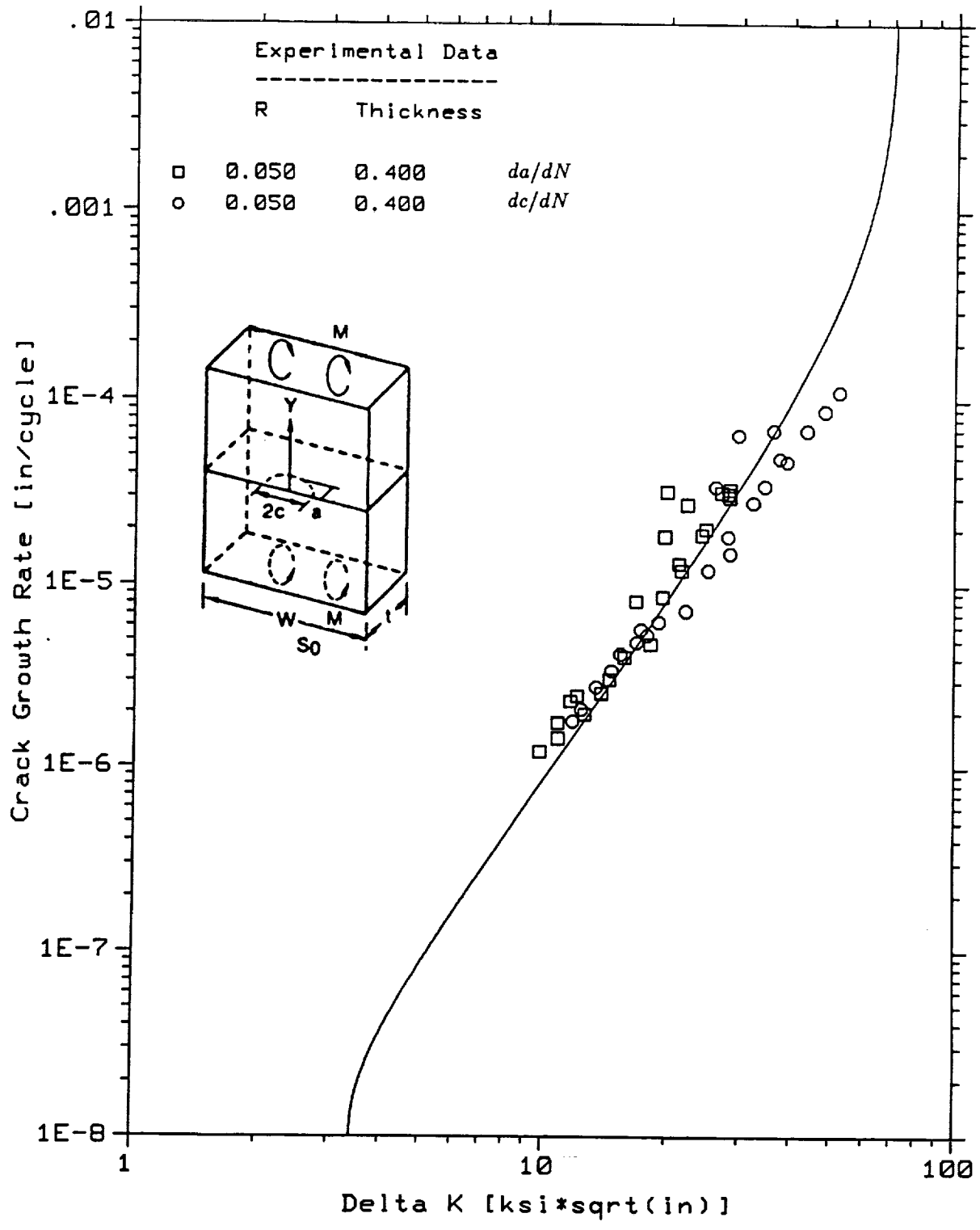


Figure 6.- Comparison of fatigue crack growth rates, surface crack in rectangular bar - three-point bending.

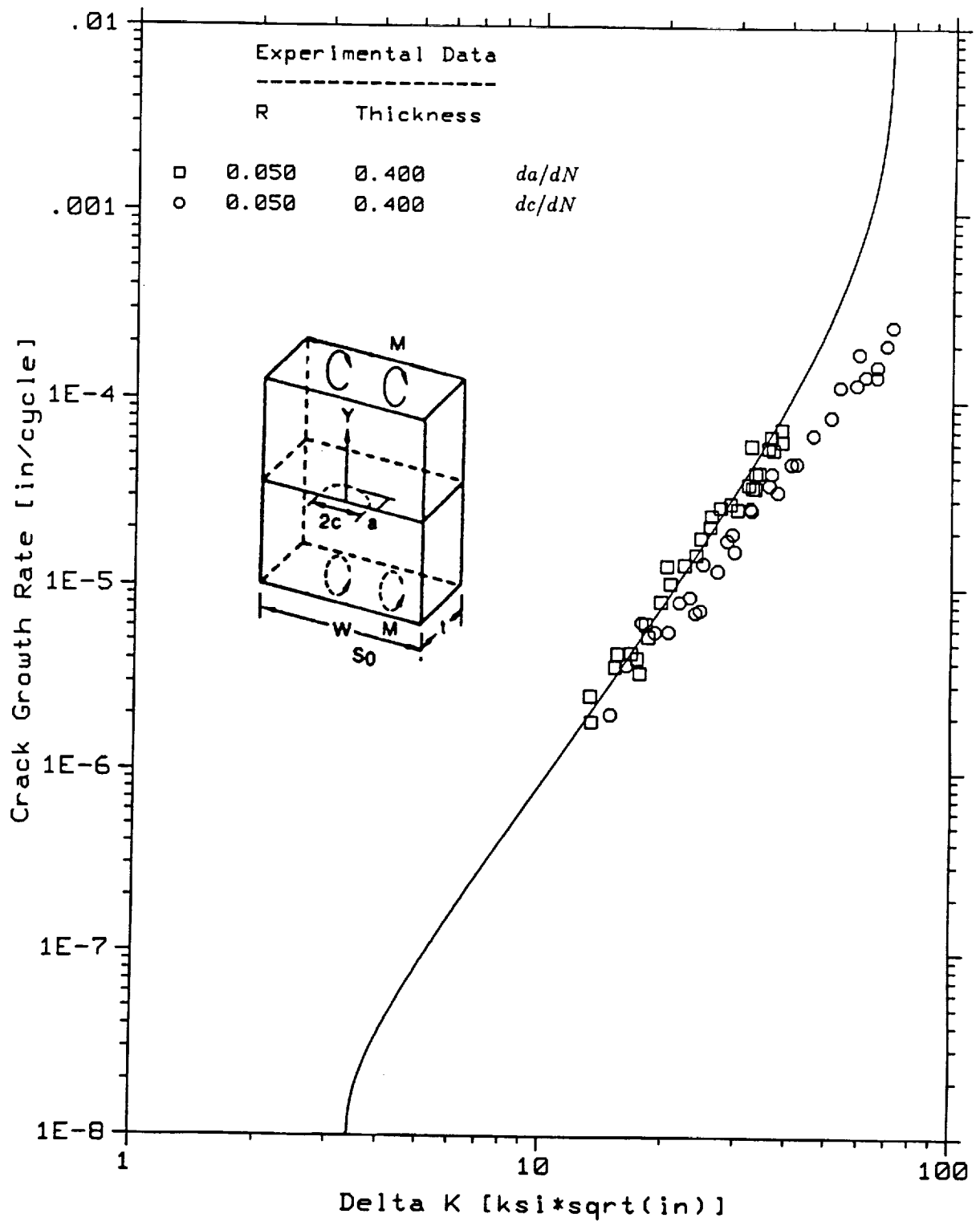


Figure 7.- Comparison of fatigue crack growth rates, surface crack in rectangular bar - cantilever bending.

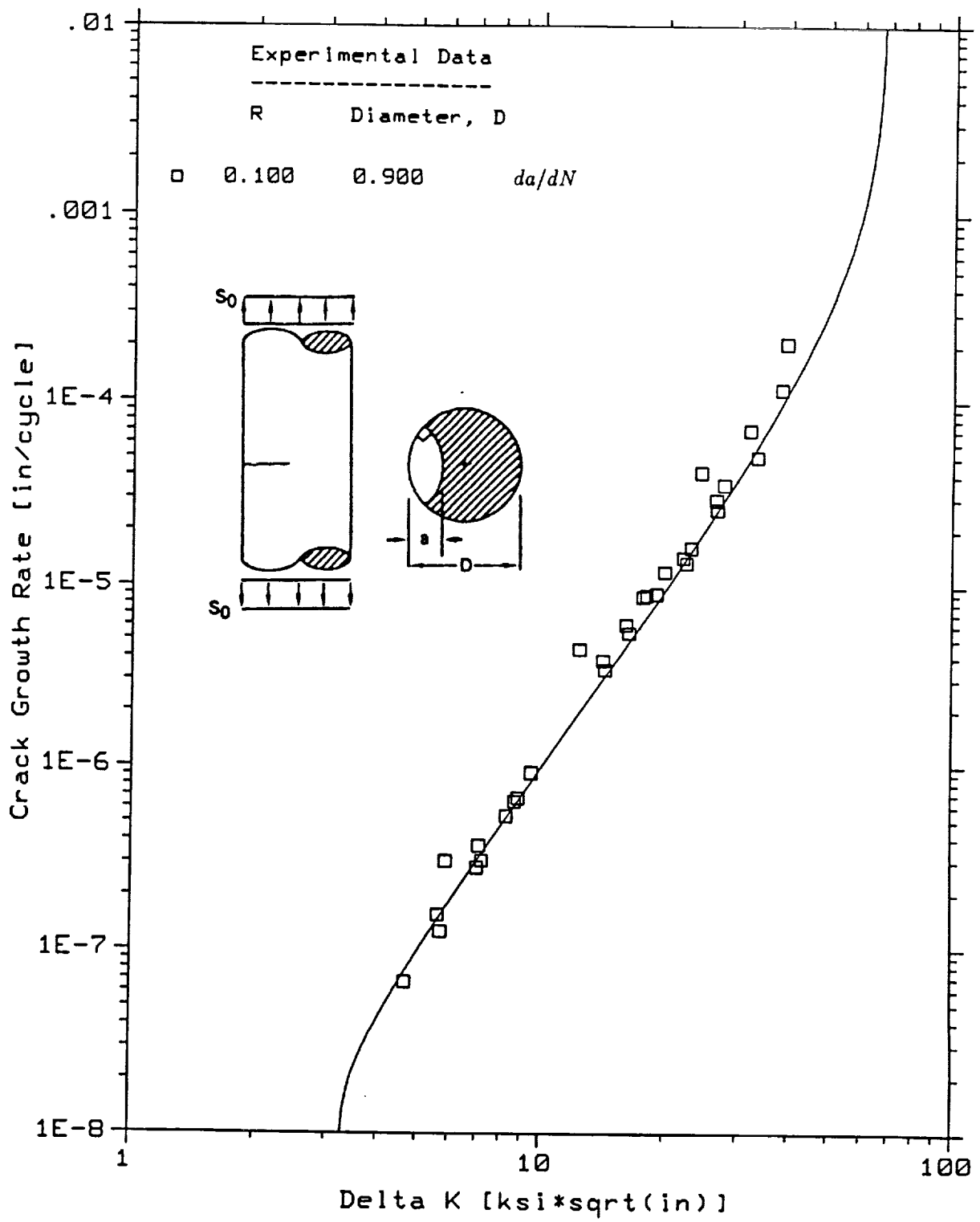


Figure 8.- Comparison of fatigue crack growth rates, surface crack in a round bar - tension.

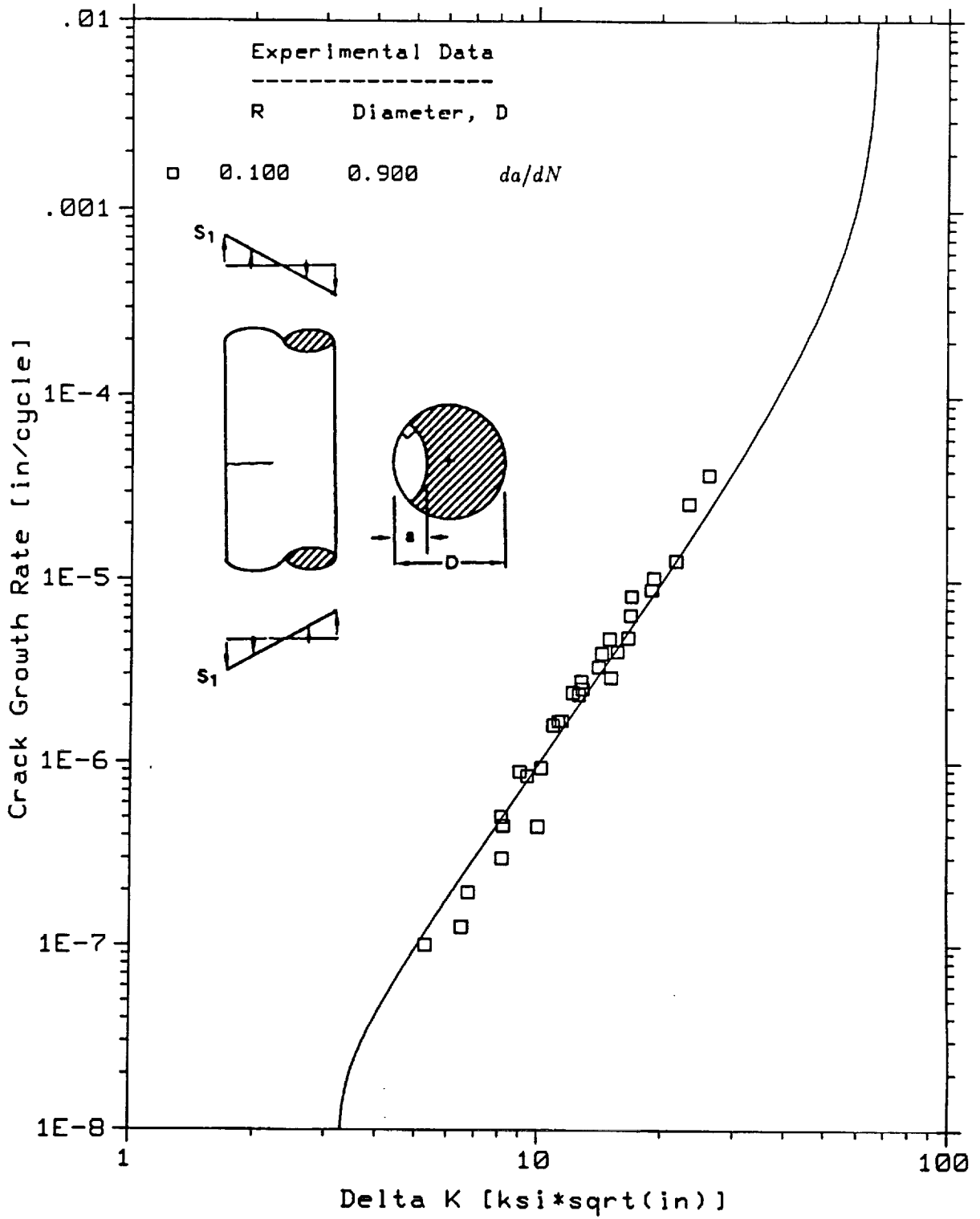


Figure 9.- Comparison of fatigue crack growth rates, surface crack in a round bar - bending.

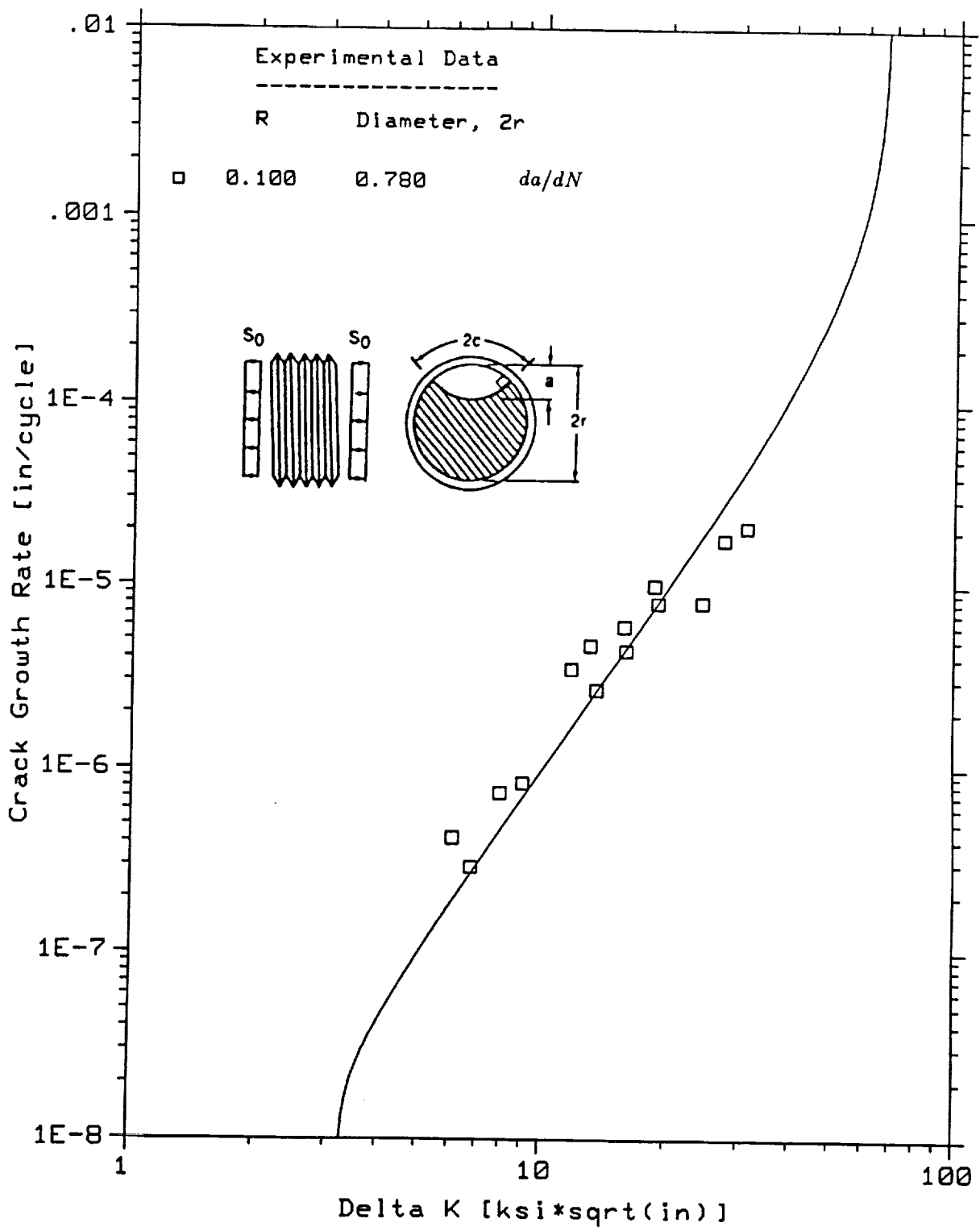


Figure 10.- Comparison of fatigue crack growth rates, surface crack in threaded round bar - tension.

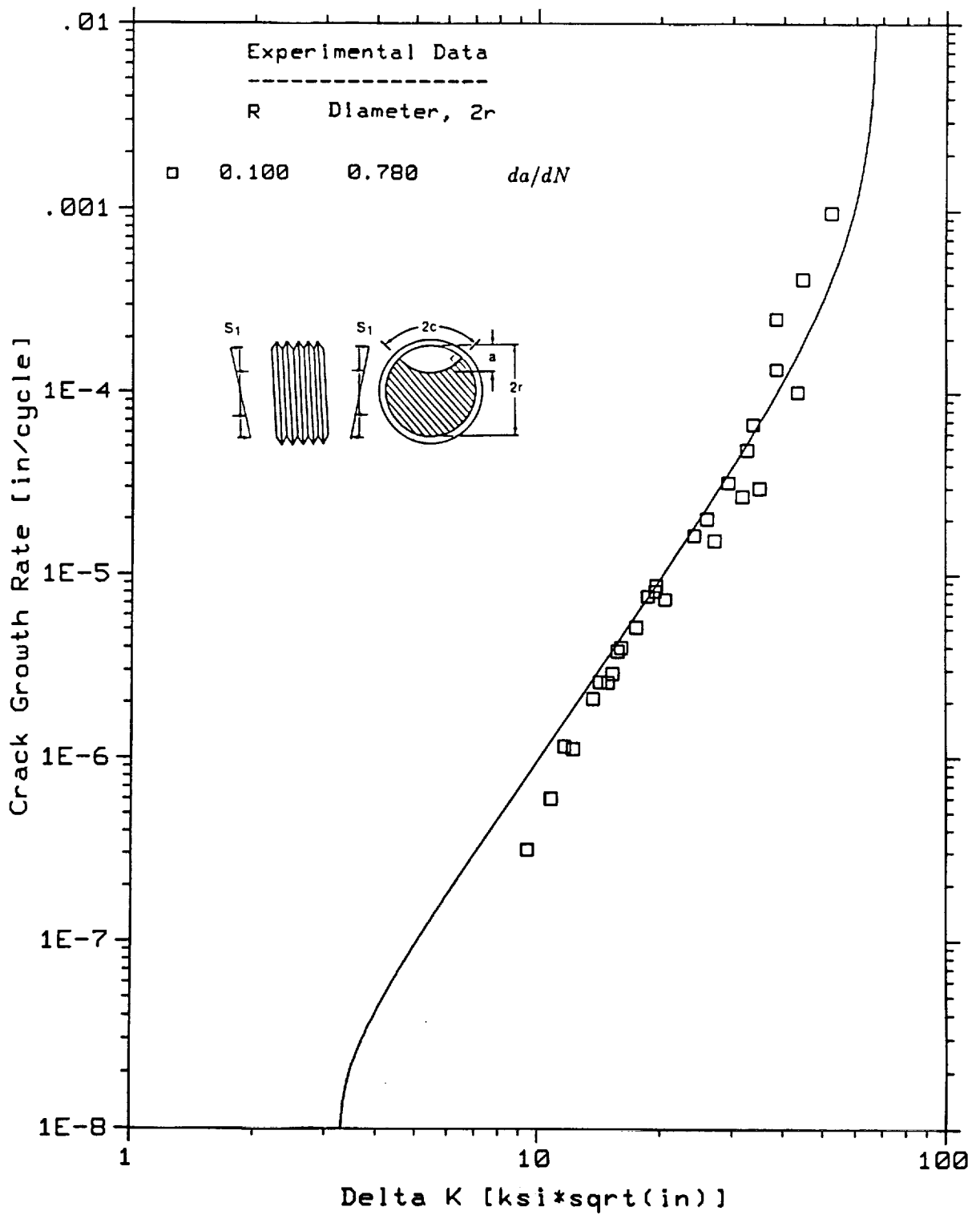


Figure 11.- Comparison of fatigue crack growth rates, surface crack in threaded round bar - bending.

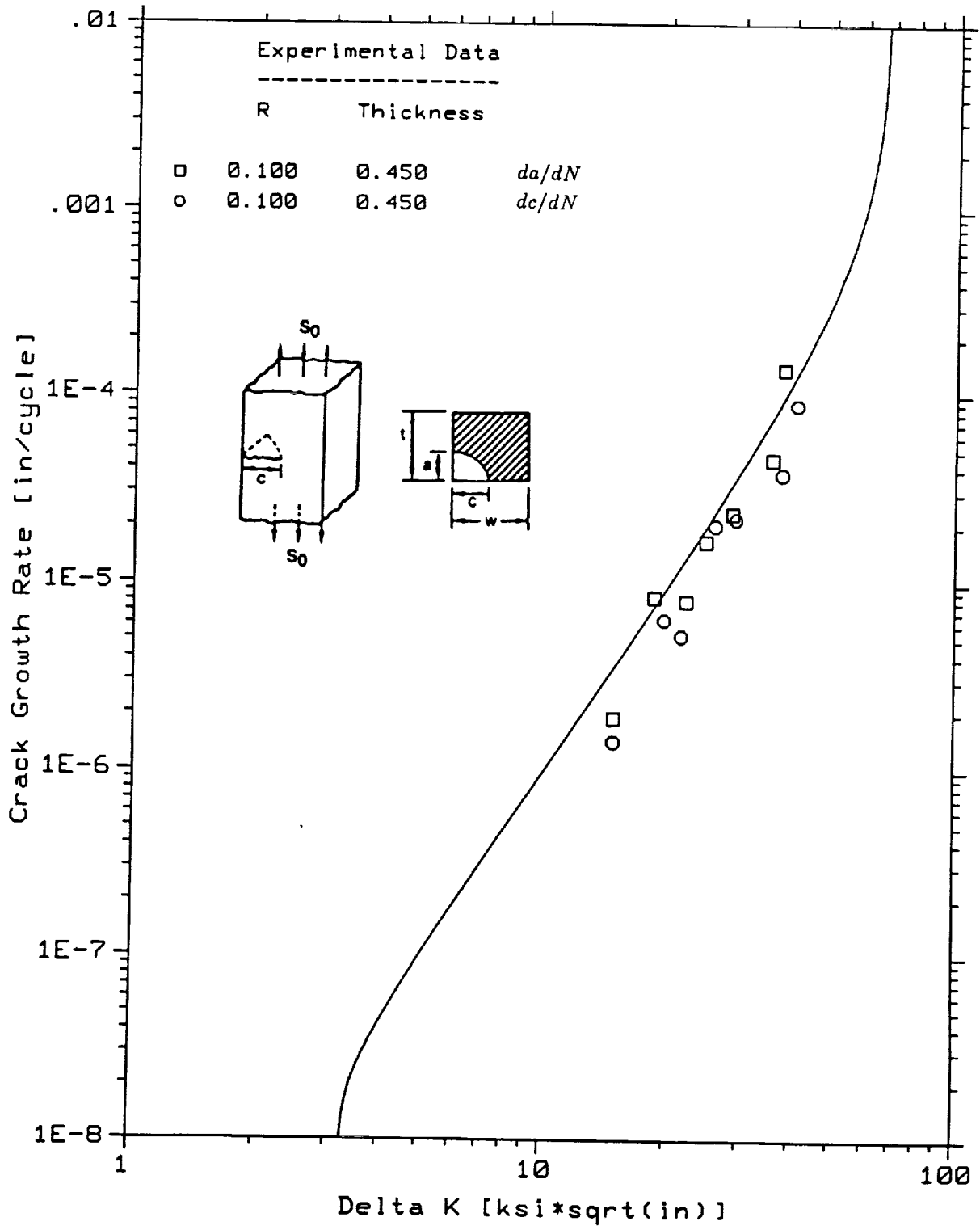


Figure 12.- Comparison of fatigue crack growth rates, corner crack in rectangular bar - tension.

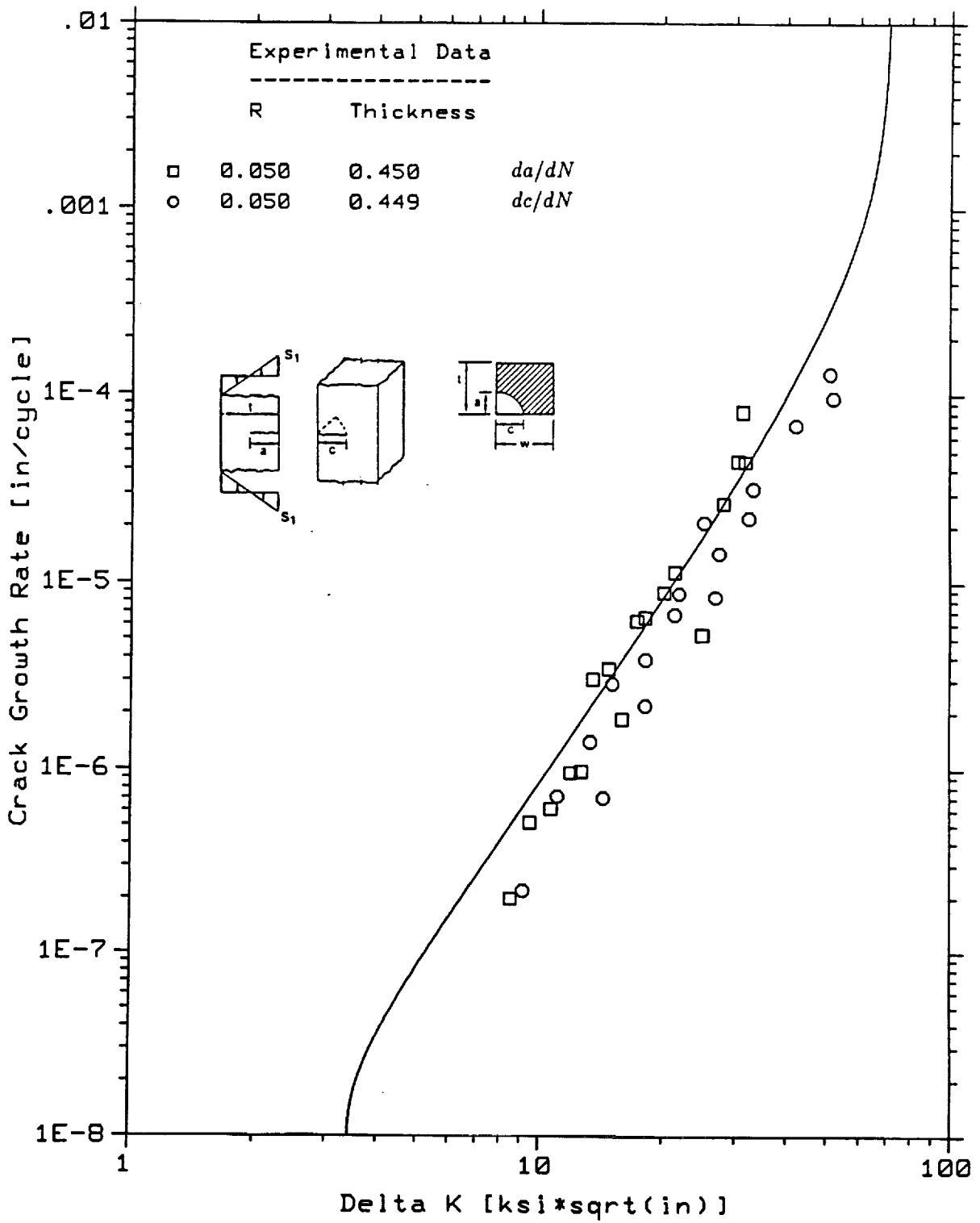


Figure 13.- Comparison of fatigue crack growth rates, corner crack in rectangular bar - bending.

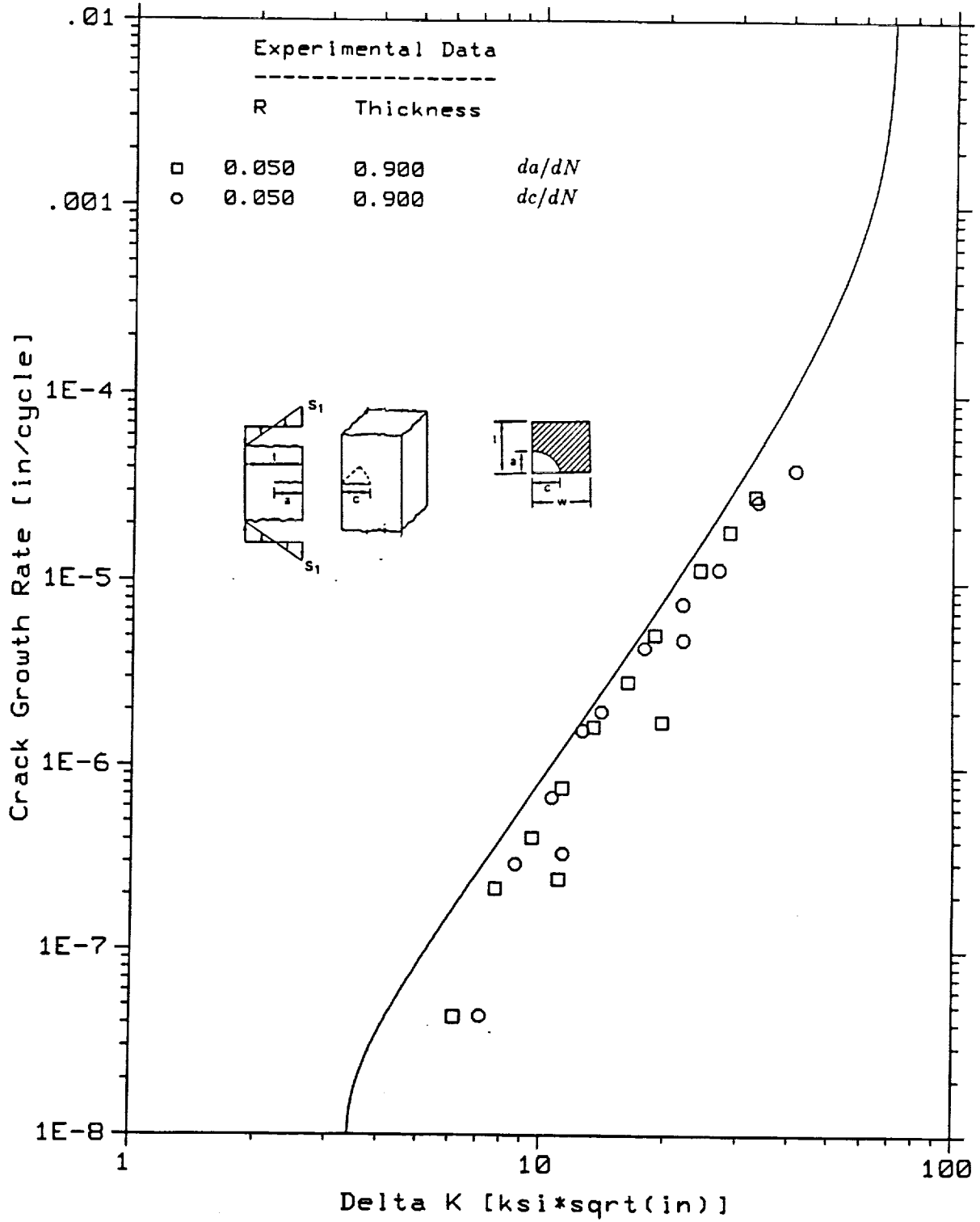


Figure 14.- Comparison of fatigue crack growth rates, corner crack in rectangular bar - bending.

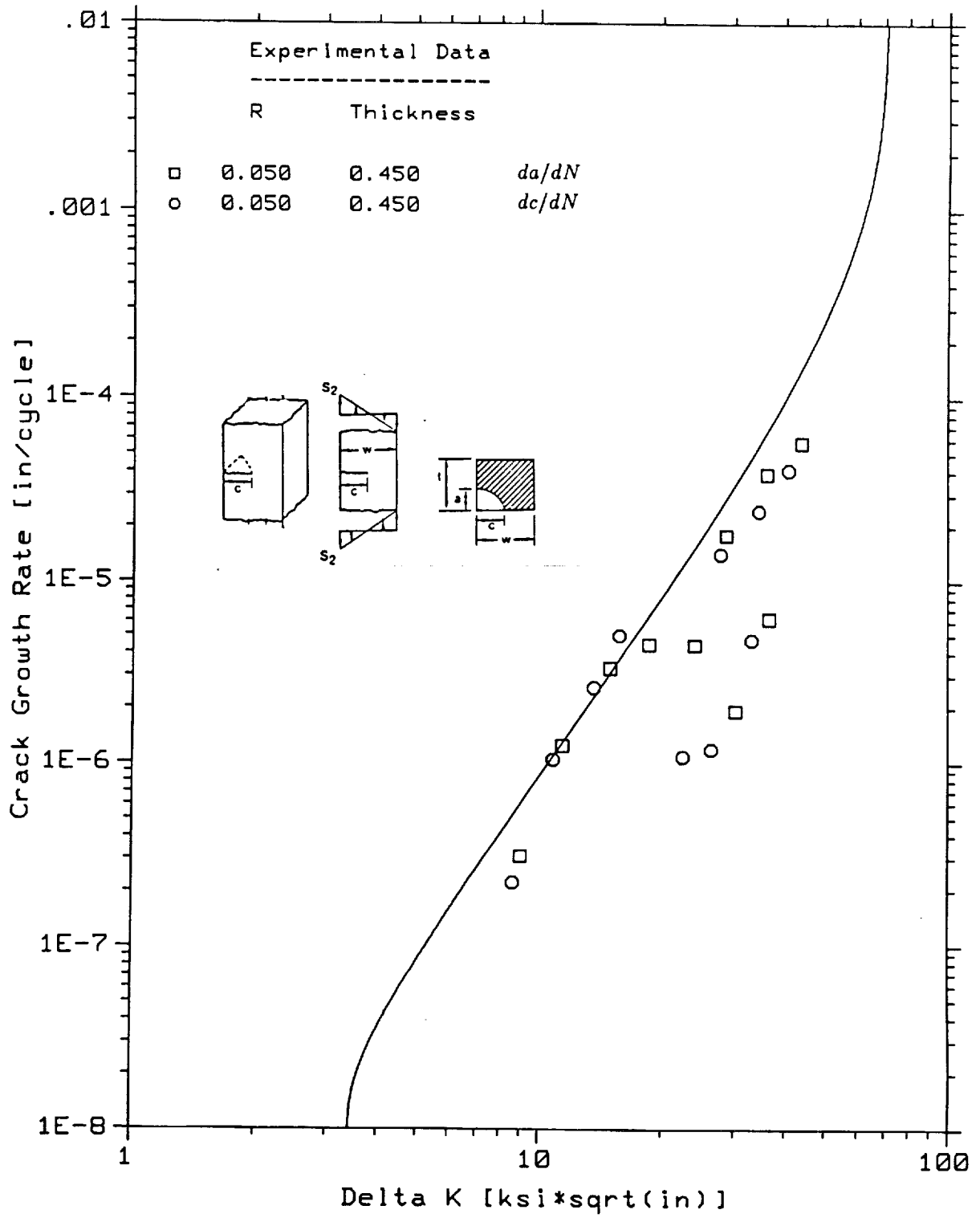


Figure 15.- Comparison of fatigue crack growth rates, corner cracked rectangular bar - transverse bending.

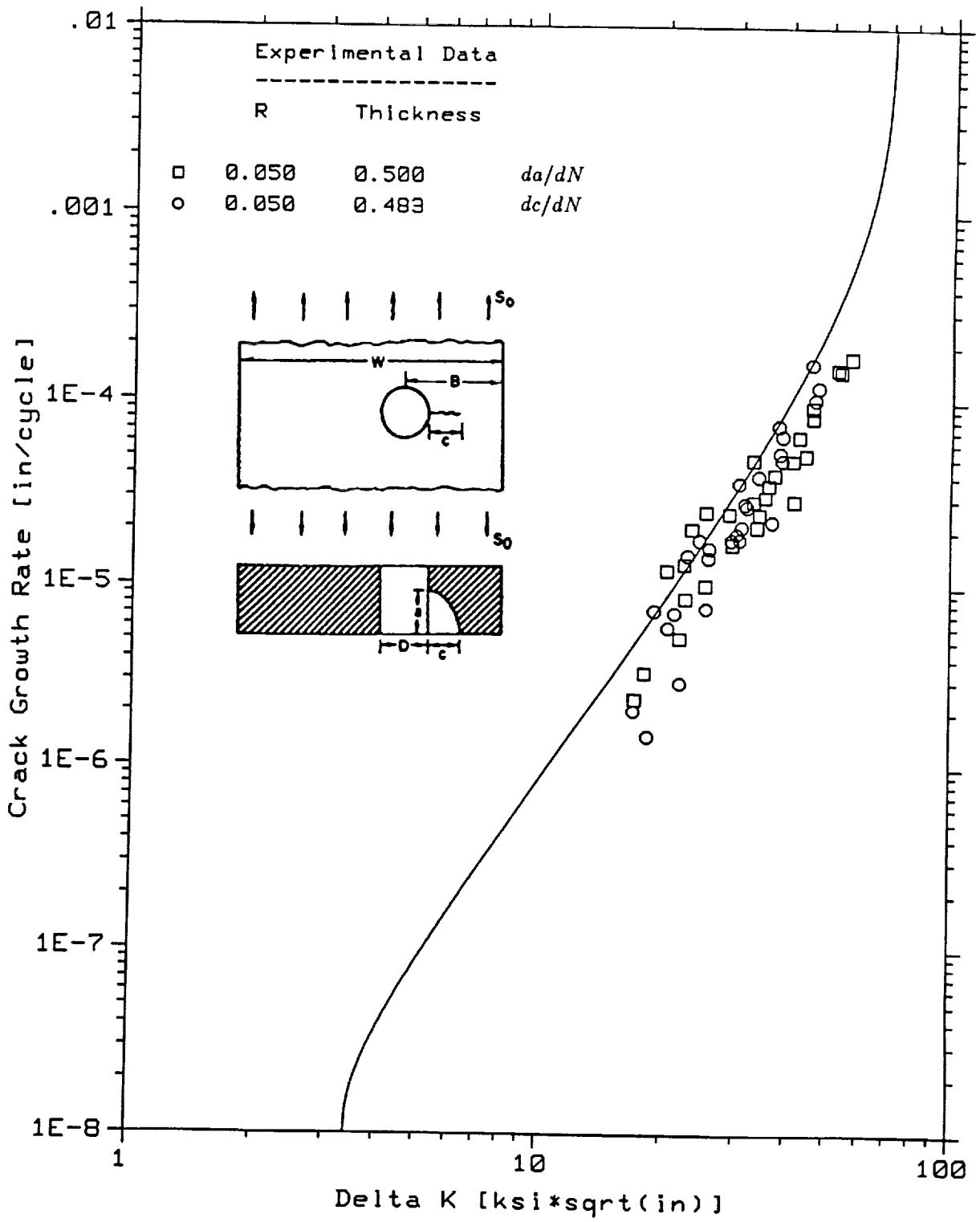


Figure 16.- Comparison of fatigue crack growth rates, corner crack from open hole rectangular bar - tension.

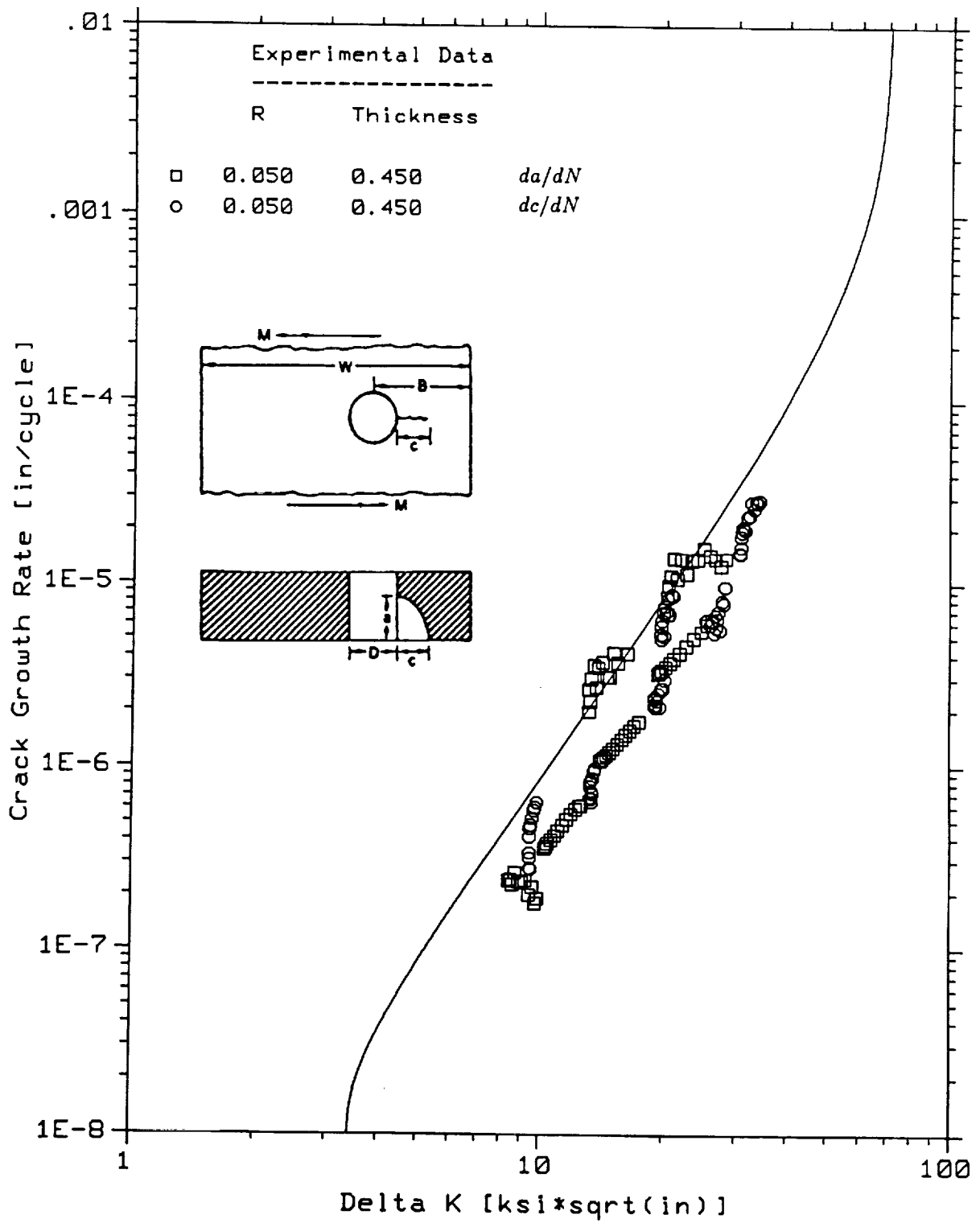


Figure 17.- Comparison of fatigue crack growth rates, corner crack from open hole, rectangular bar - 3-point bending.

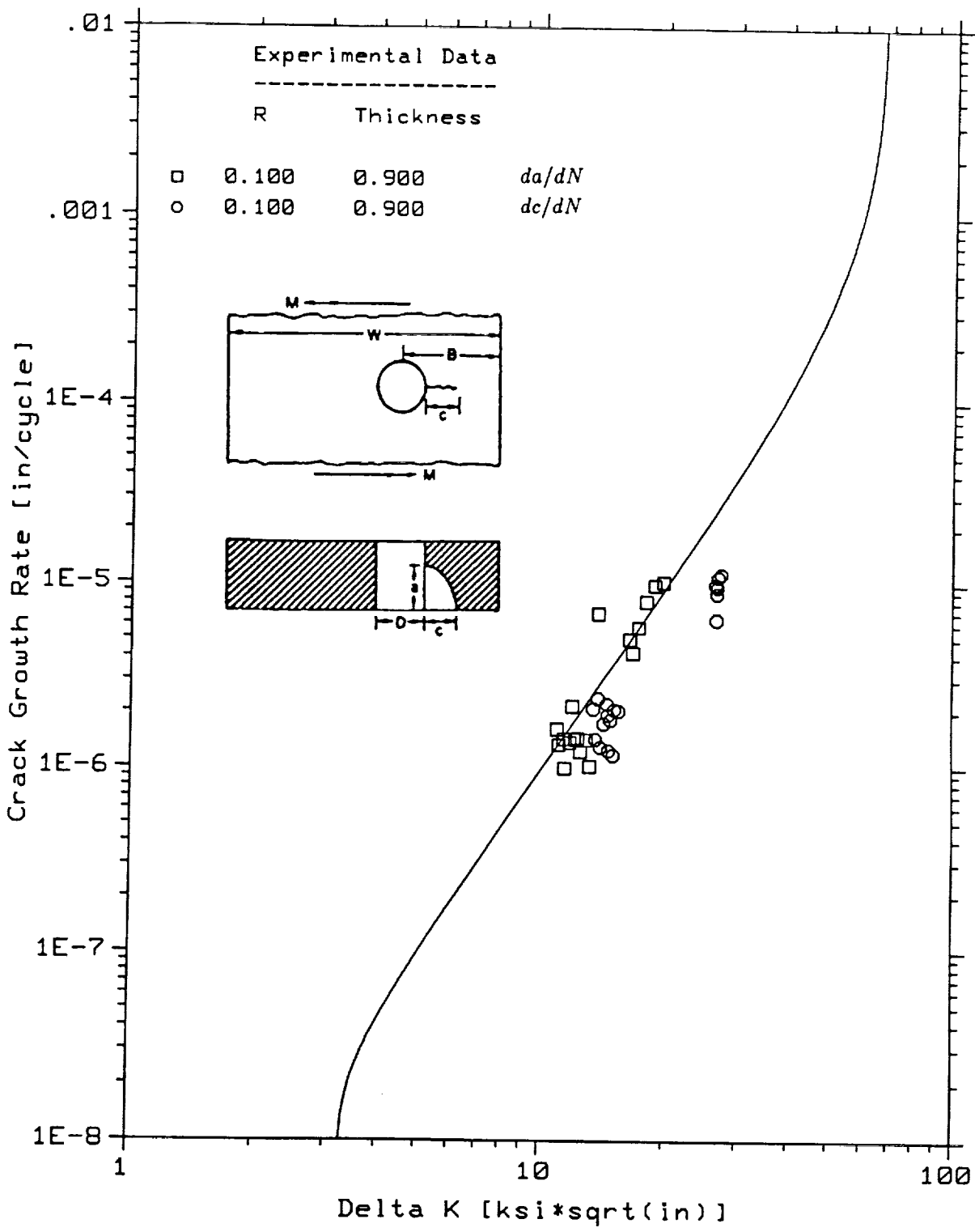


Figure 18.- Comparison of fatigue crack growth rates, corner crack from open hole, rectangular bar - 3-point bending.

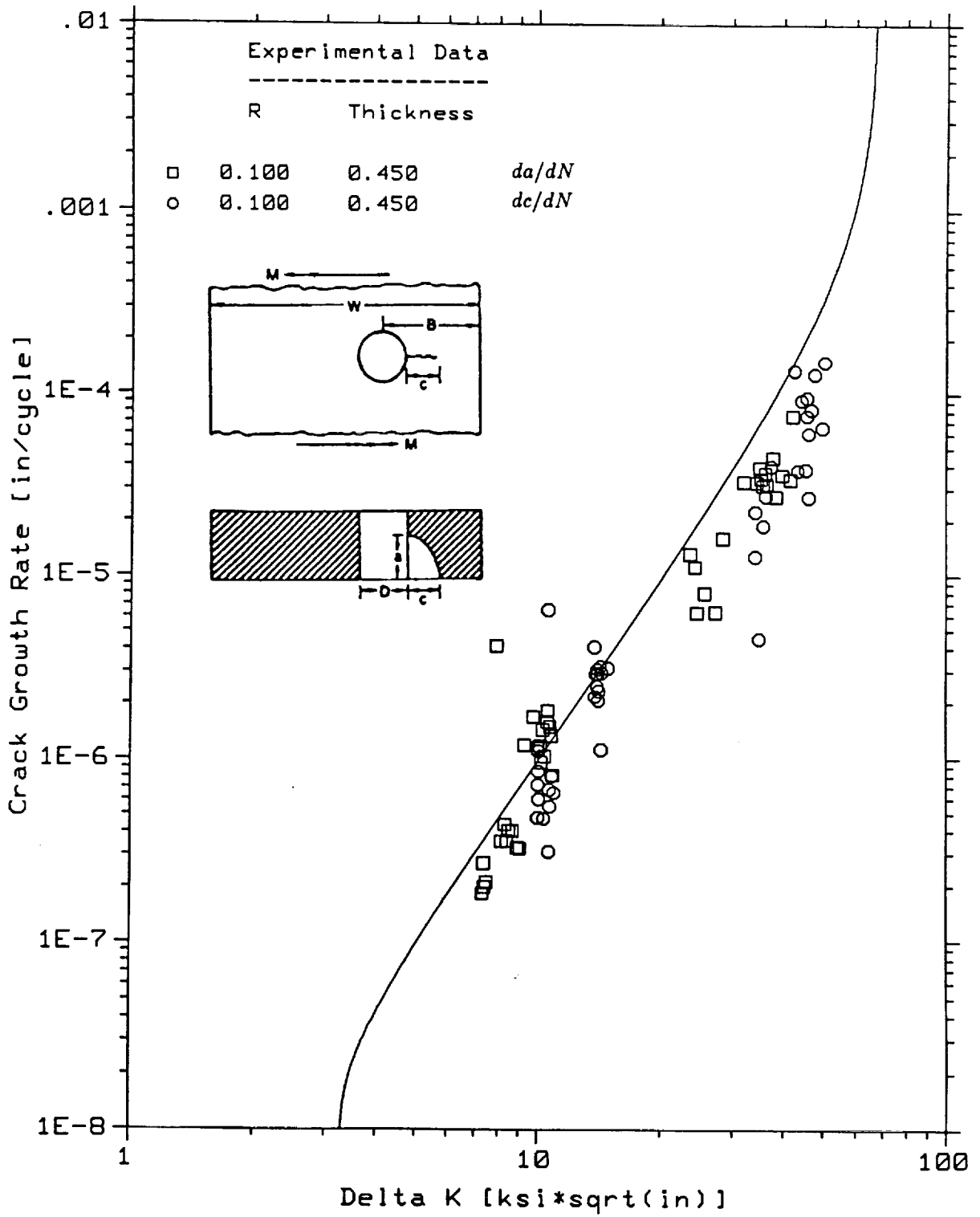


Figure 19.- Comparison of fatigue crack growth rates, corner crack from open hole, rectangular bar - 3-point bending.

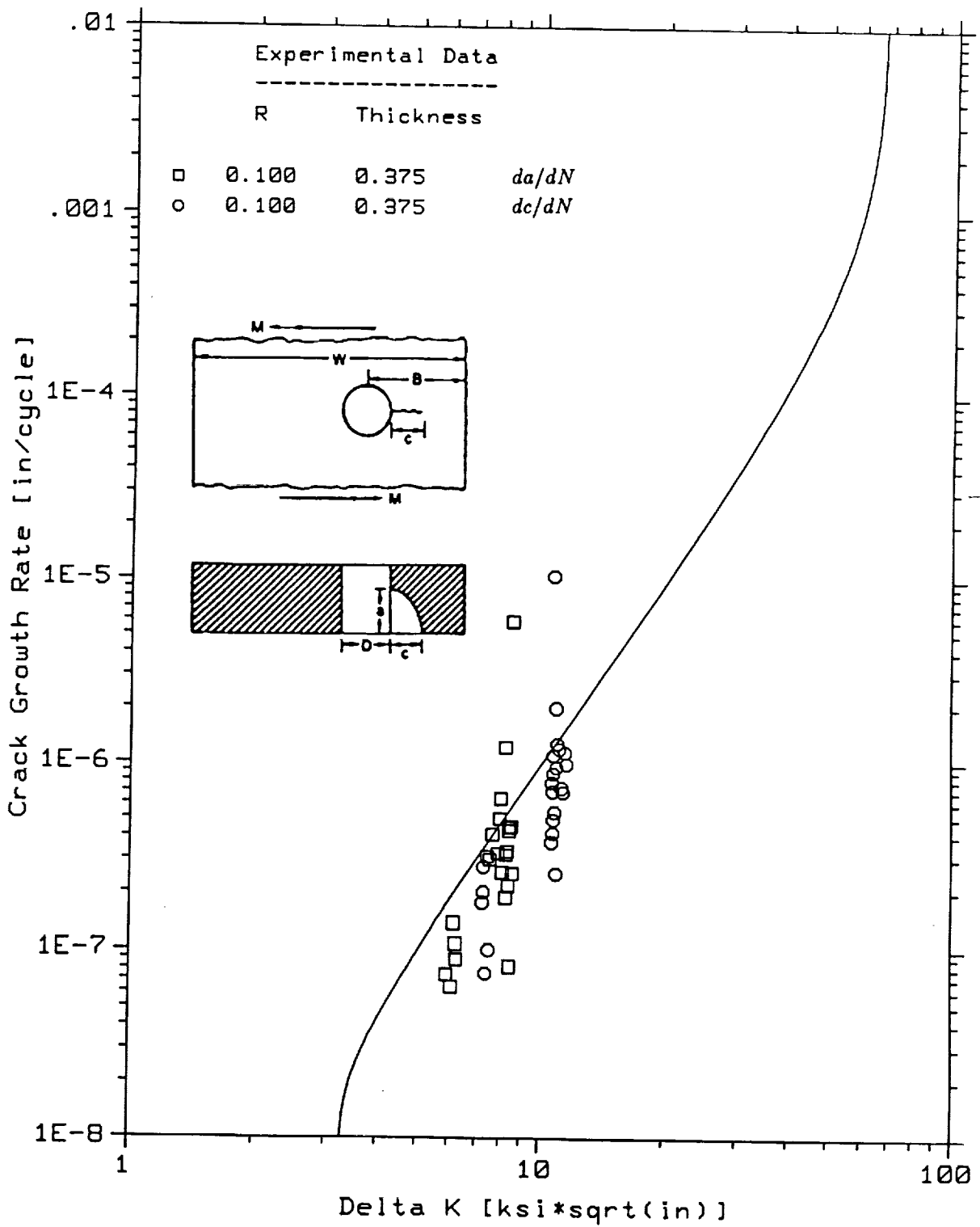


Figure 20.- Comparison of fatigue crack growth rates, corner crack from open hole, rectangular bar - 3-point bending.

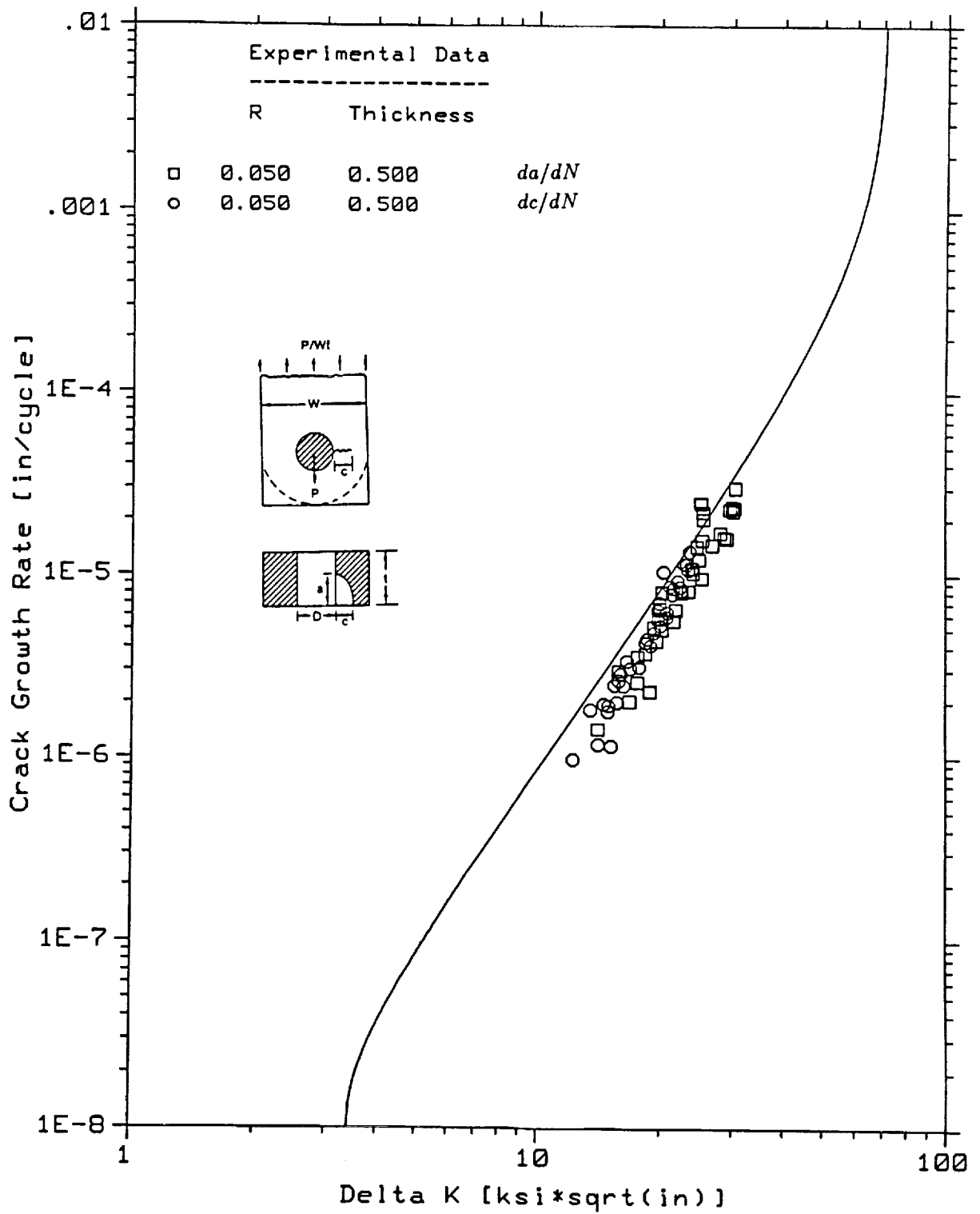


Figure 21.- Comparison of fatigue crack growth rates, corner crack from pin-loaded hole, rectangular bar.

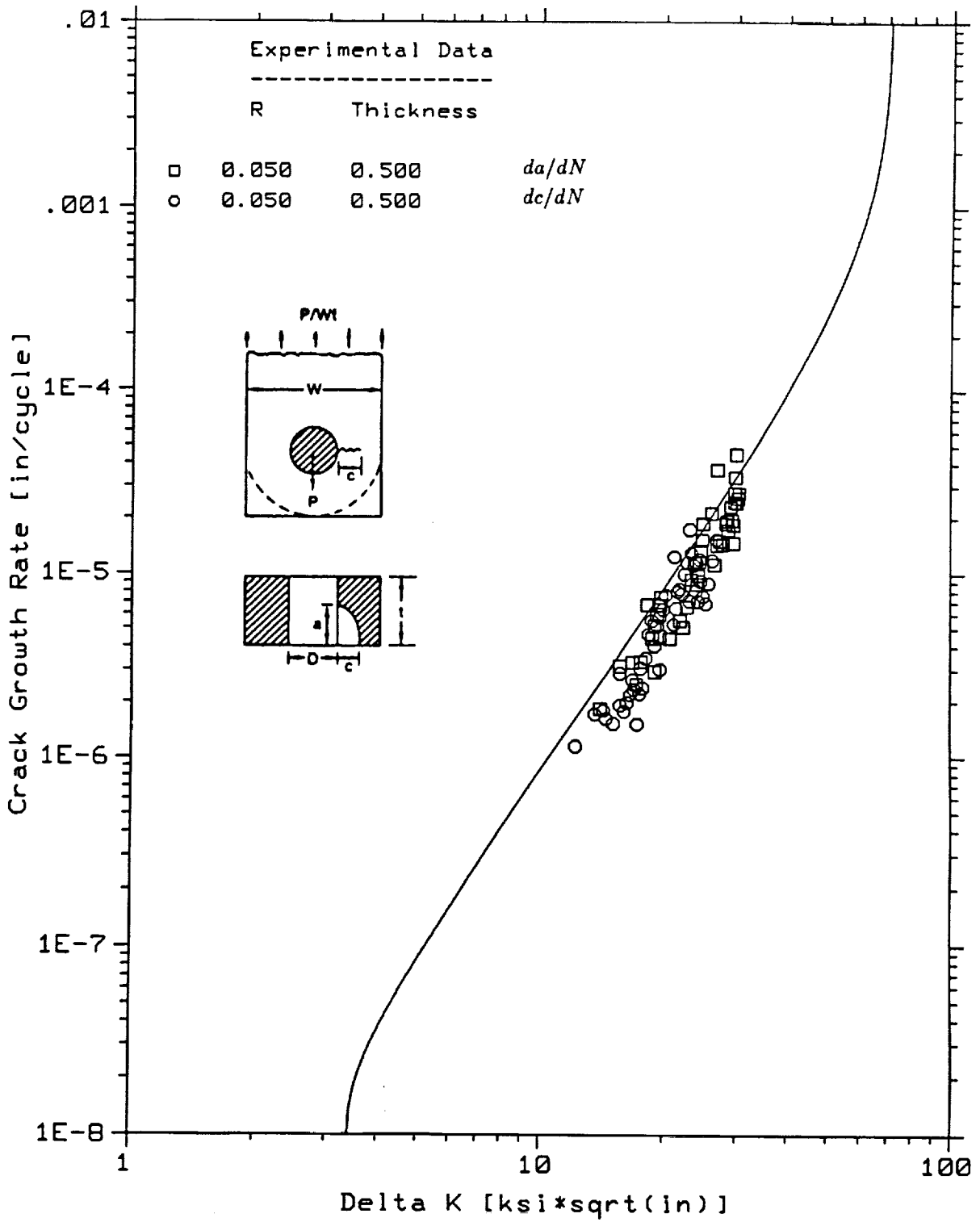


Figure 22.- Comparison of fatigue crack growth rates, corner crack from pin-loaded hole, rectangular bar.

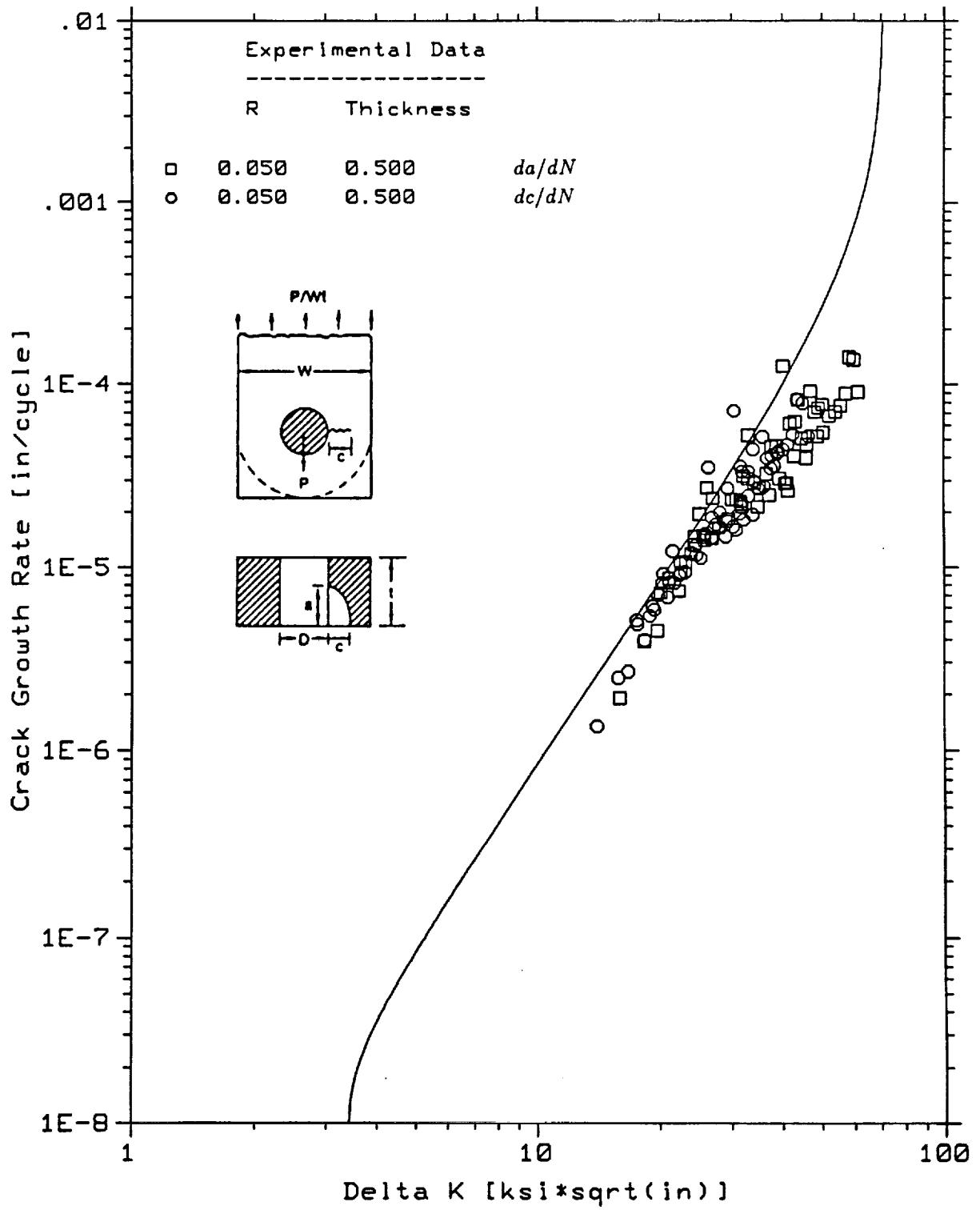


Figure 23.- Comparison of fatigue crack growth rates, corner crack from pin-loaded hole, rectangular bar.

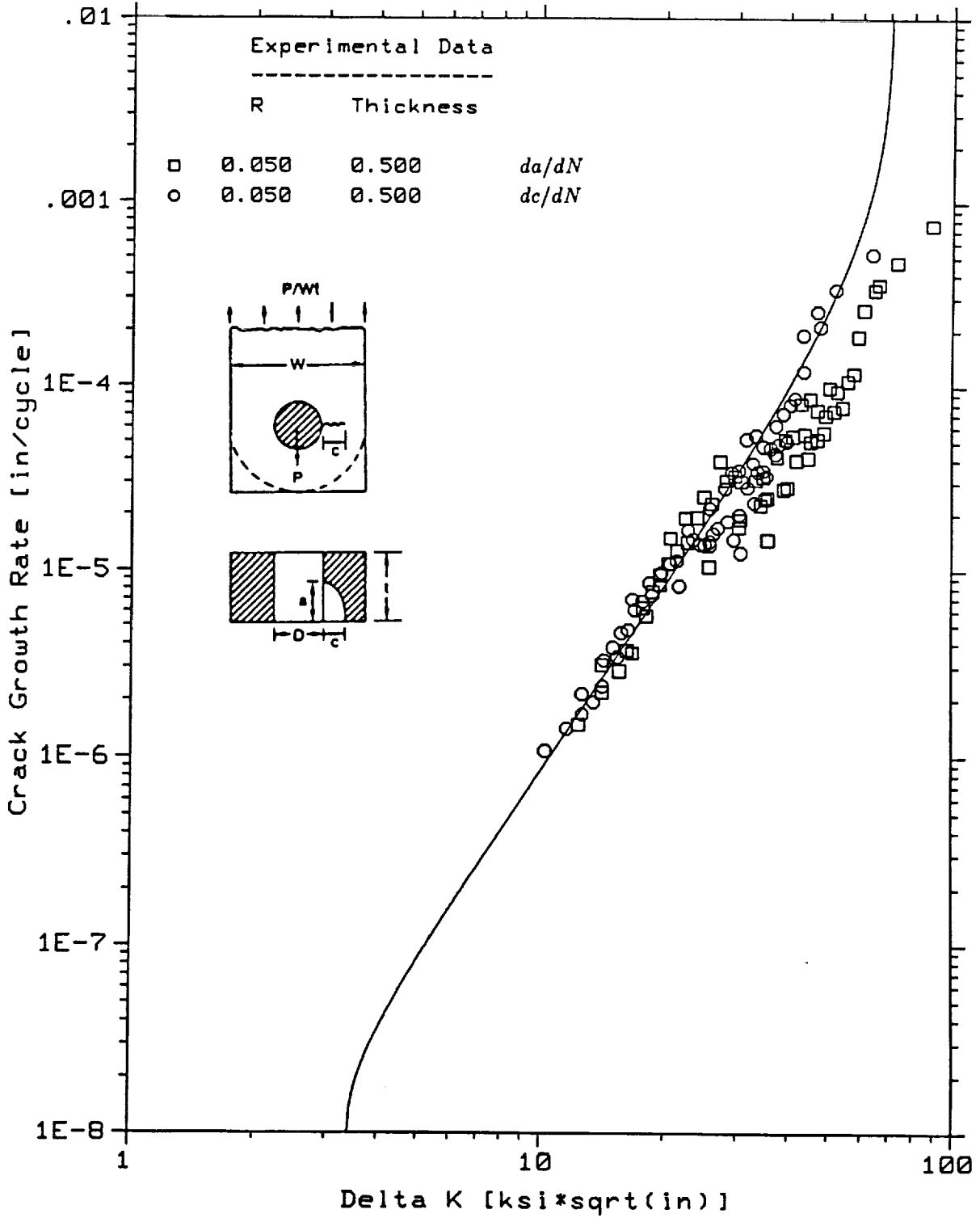


Figure 24.- Comparison of fatigue crack growth rates, corner crack from pin-loaded hole, rectangular bar.

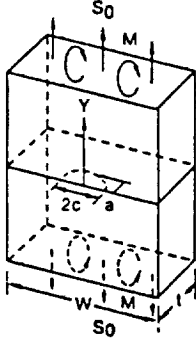
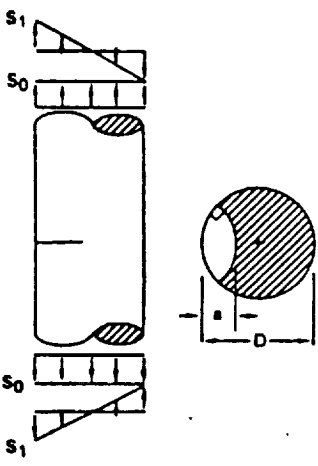
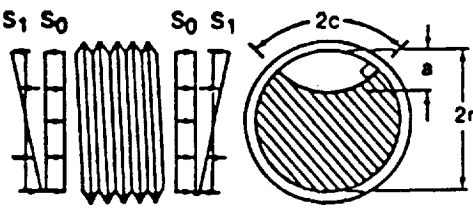
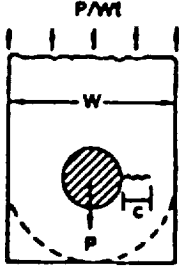
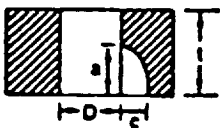
Loading	Specimen Details	Average N_t/N_e	
		Theoretical	Experimental
	Tension $W=2.8, t=0.4, R=0.05$		
	<i>a - tip</i>	1.00, 1.03, 1.31, 0.75	1.02
	<i>c - tip</i>	0.95, 1.05, 1.32, 0.79	1.03
	Bending $W=2.8, t=0.4, R=0.05$		
	<i>a - tip</i>	1.68, 1.37, 1.38, 1.20, 1.11, 1.02	1.29
	<i>c - tip</i>	1.69, 1.43, 1.35, 1.11, 1.05, 0.93	1.26
	Bending $W=2.8, t=0.4, R=0.05$		
	<i>a - tip</i>	1.04, 0.94, 1.12, 0.96, 0.76 0.66, 0.52, 1.07	0.88
	<i>c - tip</i>	1.07, 0.83, 1.07, 0.90, 0.72 0.60, 0.40, 1.07	0.83
	Tension $D=0.9, R=0.1$		
	<i>a - tip</i>	1.39, 1.11, 0.89, 1.32, 1.08, 1.27	1.15
	Bending $D=0.9, R=0.1$		
<i>a - tip</i>	1.18, 0.87, 1.19, 1.12, 0.66	1.00	
	Tension $d=0.78, R=0.1$		
	<i>a - tip</i>	0.50, 1.00, 1.66, 1.47	1.16
	Bending $d=0.78, R=0.1$		
	<i>a - tip</i>	0.81, 0.51, 0.72, 0.99, 1.02	1.16
	Pin-load $W=2.9, t=0.5, D=0.5, R=0.05$		
	<i>a - tip</i>	0.91, 1.00, 1.02	0.98
	<i>c - tip</i>	0.89, 1.03, 0.97	0.96
	Pin-load $W=1.5, t=0.5, D=0.5, R=0.05$		
	<i>a - tip</i>	0.92, 1.05, 1.10, 0.65, 0.47	0.84
	<i>c - tip</i>	0.99, 1.03, 1.11, 0.70, 0.53	0.87
	Pin-load $W=1.0, t=0.5, D=0.5, R=0.05$		
	<i>a - tip</i>	0.95, 1.57, 1.50, 0.72, 0.62	1.07
	<i>c - tip</i>	1.00, 1.56, 1.49, 0.76, 0.62	1.09

Figure 25.- Summary of life prediction results.

Loading Specimen Details		Average N_t/N_e <small>$\frac{\text{TheoreticalLife}}{\text{ExperimentalLife}}$</small>	
	Tension	$W=0.9, t=0.45, R=0.1$	
	<i>a - tip</i>	1.24, 1.26	1.25
	<i>c - tip</i>	1.23, 1.22	1.22
	Bending	$W=0.9, t=0.9, R=0.05$	
	<i>a - tip</i>	0.83, 0.89, 1.11	0.94
	<i>c - tip</i>	0.87, 0.83, 1.10	0.93
	Bending	$W=0.9, t=0.5, R=0.05$	
	<i>a - tip</i>	1.24, 1.34, 1.28, 1.11	1.24
	<i>c - tip</i>	1.24, 1.25, 1.13, 1.11,	1.18
	Bending	$W=0.9, t=0.45, R=0.05$	
	<i>a - tip</i>	1.44, 0.76	1.10
	<i>c - tip</i>	1.53, 0.75	1.14
Bending	$W=2.0, t=0.45, D=0.5, R=0.05$		
<i>a - tip</i>	0.49, 0.51, 0.51, 0.58, 1.04, 1.36	0.75	
<i>c - tip</i>	0.45, 0.48, 0.51, 0.68, 0.91, 1.24	0.71	
Bending	$W=2.0, t=0.45, D=0.5, R=0.1$		
<i>a - tip</i>	1.58, 0.84, 1.48, 0.52, 0.83		
<i>c - tip</i>	0.96, 0.58	0.97	
<i>c - tip</i>	1.34, 0.90, 1.41, 0.45, 0.83		
<i>c - tip</i>	0.90, 0.48	0.90	
Bending	$W=1.9, t=0.9, D=0.375, R=0.1$		
<i>a - tip</i>	0.97, 1.31, 0.98	1.09	
<i>c - tip</i>	0.66, 0.97, 0.87	0.83	
Bending	$W=3.0, t=0.375, D=0.75, R=0.1$		
<i>a - tip</i>	0.90, 0.71, 1.16, 1.35	1.03	
<i>c - tip</i>	0.88, 0.67, 1.03, 1.24	0.96	
Tension	$W=2.9, t=0.5, D=0.5, R=0.05$		
<i>a - tip</i>	1.24, 0.58, 0.80, 1.06, 0.84		
<i>c - tip</i>	1.96, 0.99, 1.02, 0.60	1.01	
<i>c - tip</i>	1.24, 0.54, 0.91, 1.01, 0.91		
<i>c - tip</i>	1.79, 1.01, 1.05, 0.62	1.01	

Figure 26.- Summary of life prediction results.

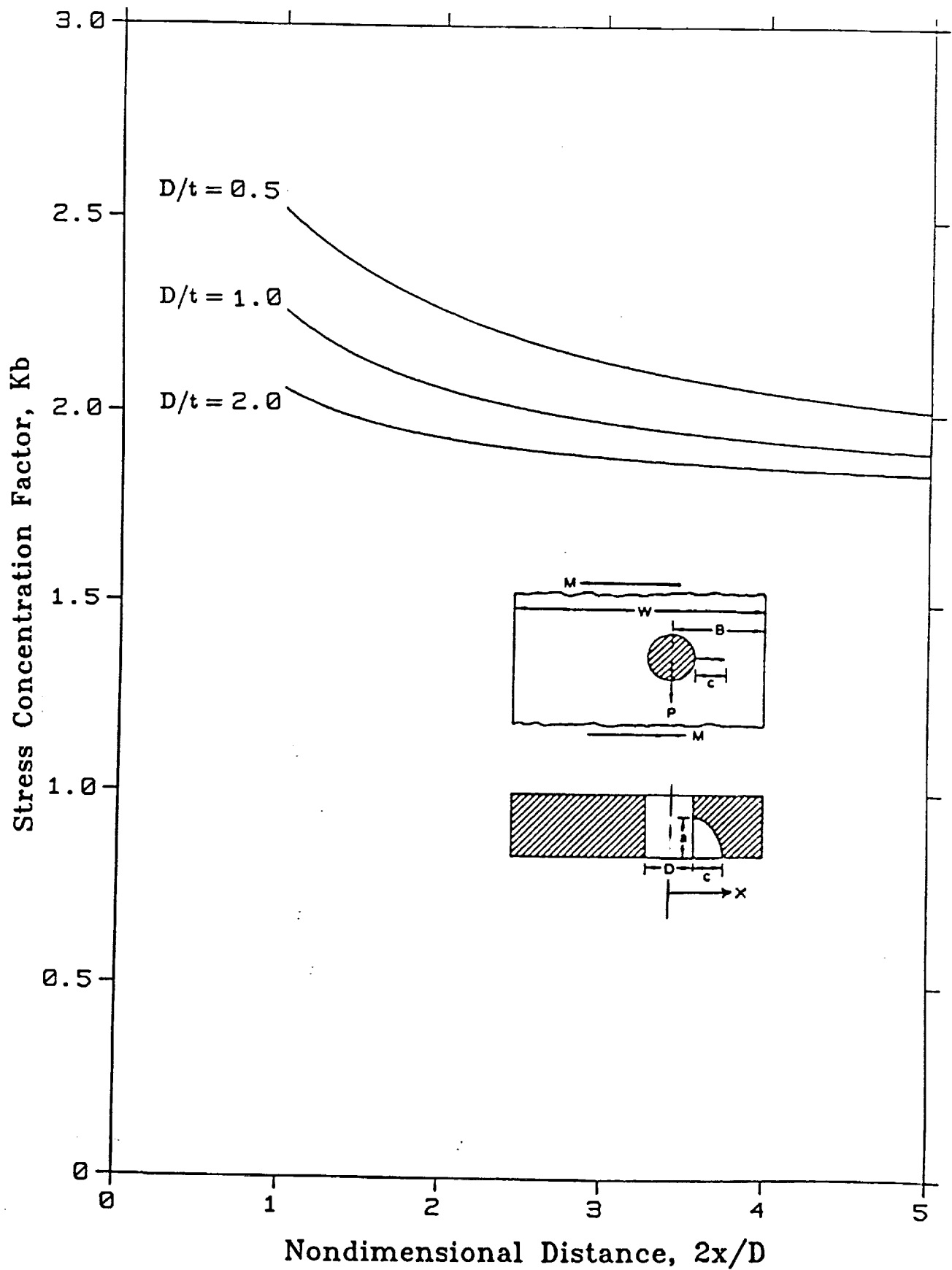


Figure 27.- Stress concentration factor for a plate with a corner crack from hole in bending.

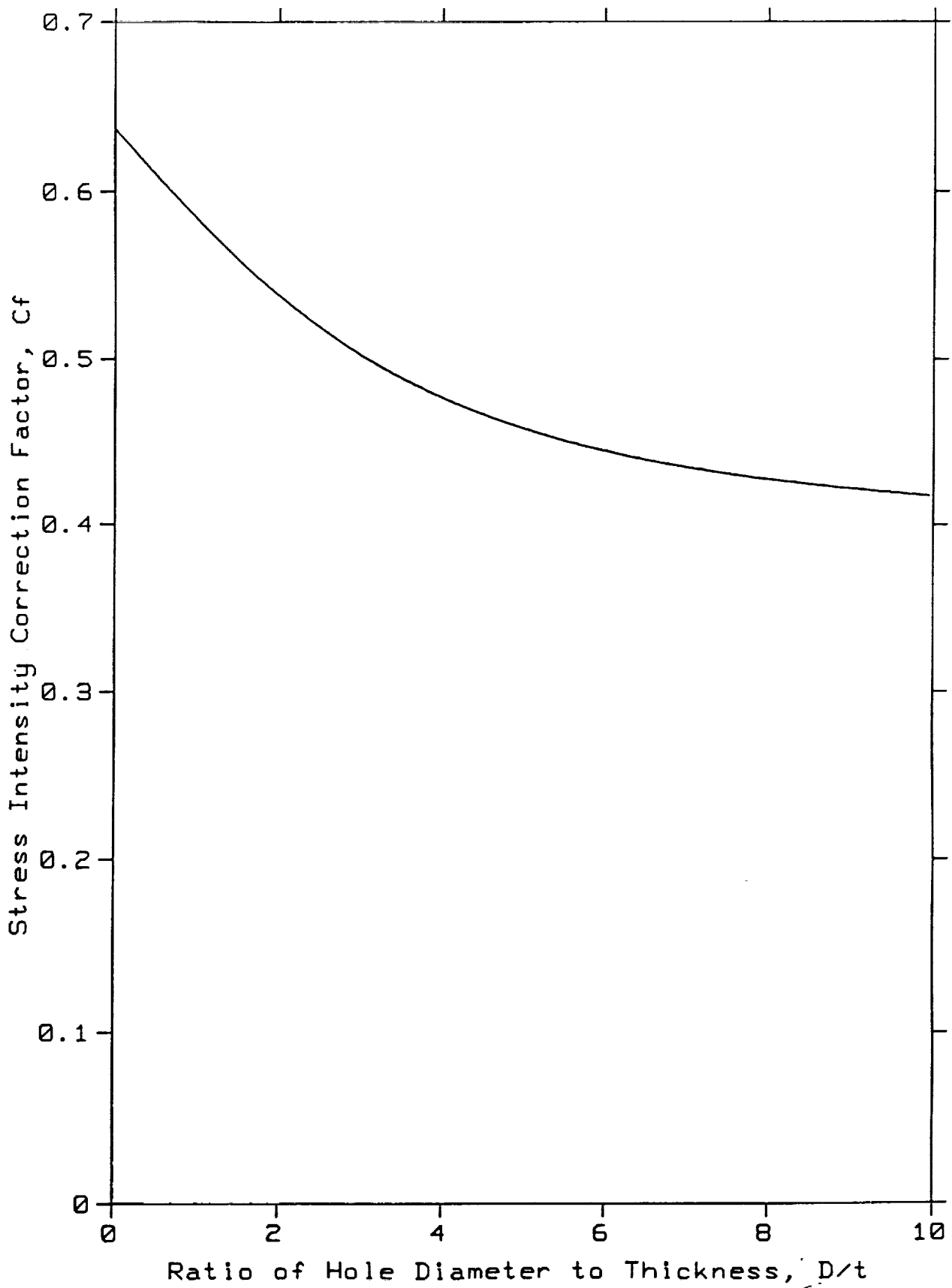


Figure 28.- Empirical stress intensity correction factor for a corner crack from hole in bending.

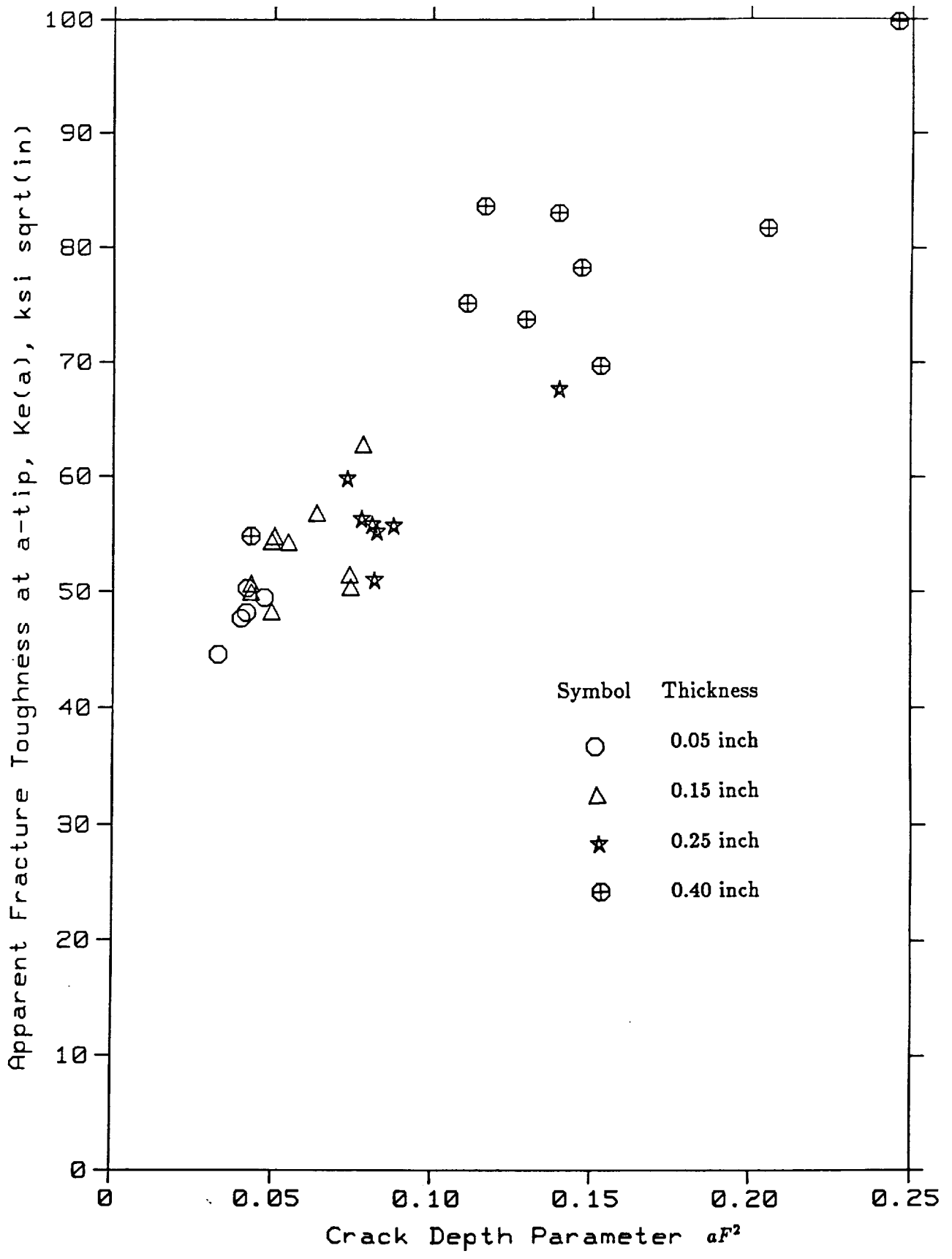


Figure 29.- Fracture toughness vs crack depth parameter for a surface crack.

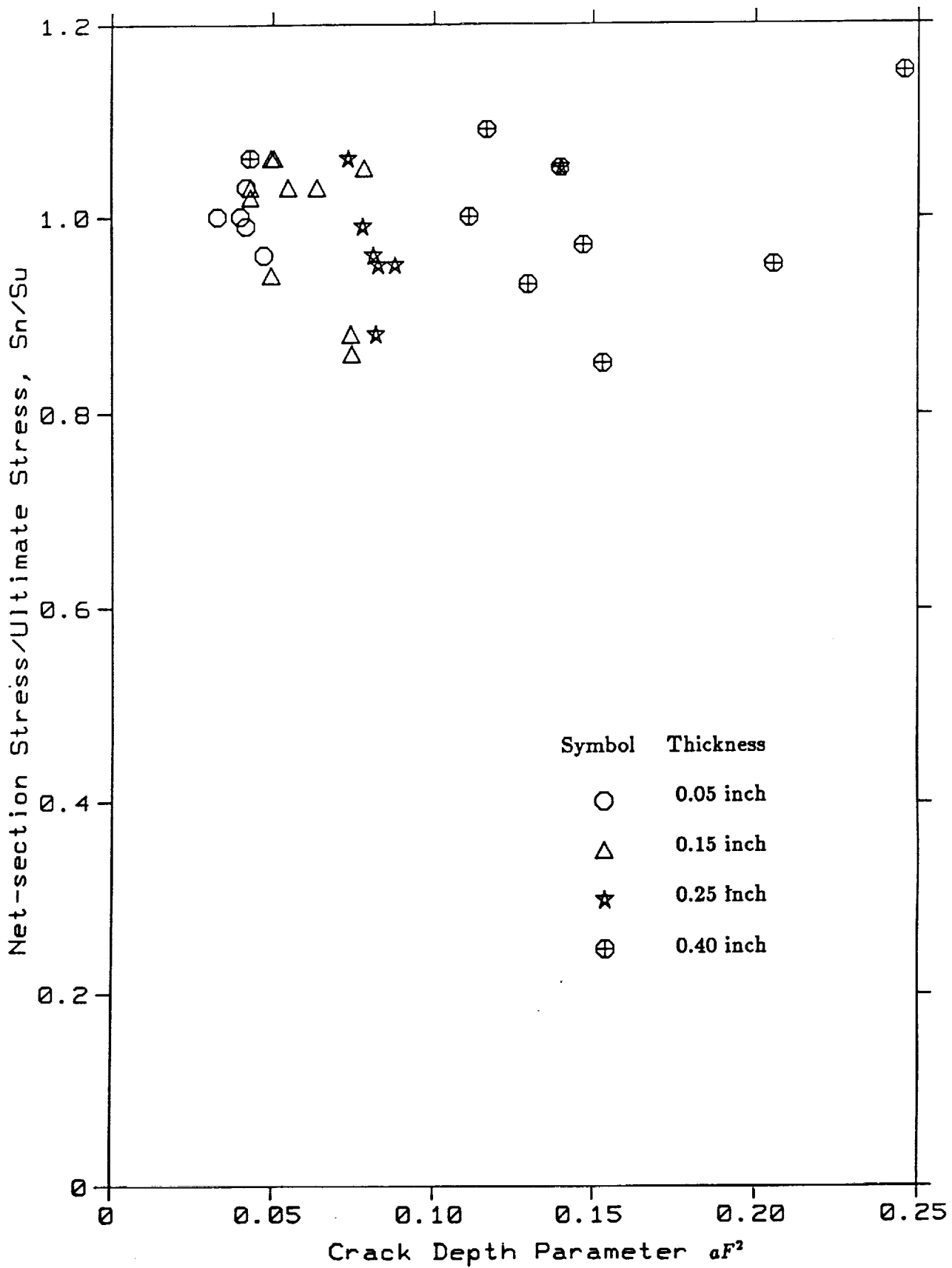


Figure 30.- Net-section stress ratio vs crack depth parameter for a surface crack.

REPORT DOCUMENTATION PAGE

1. Report No NASA TM 102165	2. Government Accession No	3. Recipient's Catalog No	
4. Title and Subtitle Behavior of Surface and Corner Cracks Subjected to Tensile and Bending Loads in Ti-6Al-4V Alloy		5. Report Date September 1990	
		6. Performing Organization Code ES5	
7. Author(s) Royce G. Forman and Sambi Metta		8. Performing Organization Report No S-611	
		9. Performing Organization Name and Address Structures and Mechanics Division Lyndon B. Johnson Space Center Houston, TX 77058	
12. Sponsoring Agency Name and Address NASA Lyndon B. Johnson Space Center Houston, TX 77058		10. Work Unit No	
		11. Contract or Grant No	
15. Supplementary Notes		13. Type of Report and Period Covered NASA TM	
		14. Sponsoring Agency Code	
16. Abstract The behavior of part-through flaws with regard to failure under monotonic loading and their growth under fatigue loading was investigated experimentally and analytically. The objective of this memorandum is to present comparisons of experimental values of toughness obtained using surface-and corner-cracked specimens with those obtained using standard test specimens, and also to compare experimental growth cycles with numerical predictions using the NASA/FLAGRO computer program. Tests were conducted on various types of surface and corner cracks under tensile and bending loads. Room temperature laboratory air provided the test environment. The material used in this investigation was the Ti-6Al-4V alloy in the solution treated and aged (STA) and stress-relieved condition. Detailed tabulation of the fracture toughness data and results of life prediction using the NASA/FLAGRO program are presented. Fatigue crack growth rates for the part-through-cracked specimens are compared with a base curve fitted from the data obtained using standard specimens. The fatigue loading used in the crack growth testing was of constant-amplitude sinusoidal type. It is concluded that the fatigue crack growth rates from standard specimens can be used with the reasonable accuracy in the case of surface and corner cracks, but the fracture toughness values from standard specimens are too conservative for the surface-and corner-crack cases.			
17. Key Words (Suggested by Author(s)) Structural Fatigue, Fatigue Crack Growth, and Fracture Toughness		18. Distribution Statement Unrestricted Subject Category 26	
19. Security Classification (of this report) None	20. Security Classification (of this page) None	21. No. of pages 59	22. Price

